JAEA-Review
2014-005

JAEA-Review

Reports on JAEA's Reimei Research Program
April 1, 2012 – March 31, 2013

(Ed.) Yuichiro NAGAME

Advanced Science Research Center

March 2014

Japan Atomic Energy Agency

日本原子力研究開発機構

本レポートは独立行政法人日本原子力研究開発機構が不定期に発行する成果報告書です。
本レポートの入手並びに著作権利用に関するお問い合わせは、下記あてにお問い合わせ下さい。
なお、本レポートの全文は日本原子力研究開発機構ホームページ（http://www.jaea.go.jp）
より発信されています。

独立行政法人日本原子力研究開発機構　研究技術情報部　研究技術情報課
〒319-1195　茨城県那珂郡東海村白方白根 2 番地 4
電話 029-282-6387, Fax 029-282-5920, E-mail:ird-support@jaea.go.jp

This report is issued irregularly by Japan Atomic Energy Agency.
Inquiries about availability and/or copyright of this report should be addressed to
Intellectual Resources Section, Intellectual Resources Department,
Japan Atomic Energy Agency.
2-4 Shirakata Shirane, Tokai-mura, Naka-gun, Ibaraki-ken 319-1195 Japan
Tel +81-29-282-6387, Fax +81-29-282-5920, E-mail:ird-support@jaea.go.jp

JAEA-Review 2014-005

Reports on JAEA's Reimei Research Program
April 1, 2012 – March 31, 2013

(Ed.) Yuichiro NAGAME

Advanced Science Research Center
Japan Atomic Energy Agency
Tokai-mura, Naka-gun, Ibaraki-ken

(Received January 9, 2014)

The Reimei (Dawn) Research Program is conducted based on public application to encourage original and/or unique ideas in the field of new frontier research on atomic energy sciences. Candidates for the offering have been extended beyond the country since the fiscal year of 2010. The seven research subjects including two ongoing ones were accepted in the fiscal year 2012 that were carried out in collaboration with Advanced Science Research Center. The three successive projects, in particular, have achieved substantial progress through the effective international collaboration. The summaries of these research subjects are compiled in this report.

We hope that new frontier research projects will be developed through the present Reimei Research Program.

Keywords: Reimei Research Program, Atomic Energy Science

JAEA-Review 2014-005

平成 24 年度黎明研究成果報告集

日本原子力研究開発機構　先端基礎研究センター
（編）永目　諭一郎

（2014 年 1 月 9 日受理）

原子力科学の分野で革新的な原理や現象の発見をめざす先端基礎研究を対象として、研究テーマを原子力機構外から公募する黎明研究制度が平成 18 年度から新たに発足した。研究期間を最長 2 年間とし、年度ごとに評価を実施して課題を採択することとした。平成 22 年度からは応募対象を国外にも広げ、国際共同研究へと発展させている。平成 24 年度は、応募総数 18 件の中から継続課題 2 件を含む 7 件を選定し、先端基礎研究センターとの共同研究として実施した。特に継続の 3 課題は大きな進展を遂げており、国際共同研究による研究交流が効果的に機能している。

本報告書は、黎明研究から多くの基礎・基盤研究が進展する一助とするため、黎明研究の実施者より提出された成果報告書をまとめ、公表するものである。

原子力科学研究所（駐在）：〒319-1195　茨城県那珂郡東海村白方白根 2-4

平成24年度黎明研究事後評価
Post-Evaluation of the REIMEI research conduted in 2012

平成25年3月15日に開催された平成24年度黎明研究評価委員会において、各課題代表者が研究成果発表を行った。
以下は、黎明研究評価委員による総評である。
The research results of each project were presented at the Reimei Evaluation Meeting (FY2012) on March 15, 2013. Below are overall evaluations given by the Evaluation Committee.

	Principal Researcher	Reseraach Theme	Grade	Review
1	Christoph E. Düllmann	Gas-phase chemistry of Sg(CO)6 – Establishing novel metal-organic chemistry for superheavy elements	S	挑戦的な研究に国際的連携で取り組んでおり、興味深い成果があがっていると認められる。 The challenging research has been carried out under the international collabration. Intersting results have been produced.
2	Gerrit E.-W. Bauer	Theory for spin engines	S	スピン-軌道相互作用が誘起する新奇な物性について著しい成果をあげており、フロンティアを開拓している。 Significant outcomes have been obtained on novel physical properties induced by spin orbit interaction. The project has been pushing the frontieres of the research field.
3	青木　大	異方的な磁気ゆらぎで探るアクチノイド化合物の重い電子系超伝導	S	アクチノイド化合物の物理について、精力的な研究により多くの重要な成果が出ており、高く評価される。今後、μSRなどの新たな実験手法を巻き込んだ展開や他の物質への波及を期待する。 The project is valued for many important results achieved through the enthusiastic research on physics of actinide compounds. Expected developments are, namely, involvements of new experimental maneuvers, e.g. using μSR, and making impact on other materials.
4	Elvezio Morenzoni	Muon spin relaxation studies of Skyrmion Spin Systems and Magnetic Semiconductors	S	強力な国際研究グループを構成し多角的な研究を進めており、確実な成果をあげている。 This is a very powerful international research collaboration team. The outstanding results has been obtained.
5	Marie-Anne Herve du Penhoat	Initial processes of radiation effects on genomic stability	A	興味深いテーマの研究だが、研究の進捗状況や成果があまり見られなかったのが残念。 Although the research theme is interesting, either remarkacle progress or new results were not clear in the presentation. It is expected that they will be described in the final report.
6	Andrei Andreyev	New island of asymmetric fission in proton-rich nuclei	S	多くの成果をあげていることが認められる。Andreyevをグループリーダーに迎えたことで、研究がさらに発展していくことを期待する。 Many results have been achieved. Having Andreyev as a group leader, further progress is expected.
7	Lynne Macaskie	Exploration of biological specific function by heavy elements stimulus	A	よい研究協力により進められていることがうかがえる。成果が福島の問題に活かされることを期待する。 The good research collaboration has been in progress. The results are expected to be used for the Fukushima restoration.

【評定基準】

S:特筆すべき成果が認められる Distinguished　A:予想された以上の成果が認められる Excellent　B:予想された成果が認められる Satisfactory　C:予想された成果が認められない Unsatisfactory

Contents

目次

This is a blank page.

1. $Sg(CO)_6$ – The First Organometallic Transactinde Complex Opening a Window to a New Compound Class

J. Even[1], A. Yakushev[2], Ch.E. Düllmann[1,2,3], H. Haba[4], M. Asai[5], T. Sato[5], H. Brand[2], A. Di Nitto[3], R. Eichler[6,7], F. L. Fan[8], W. Hartmann[2], M. Huang[4], E. Jäger[2], D. Kaji[4], J. Kanaya[4], Y. Kaneya[5], J. Khuyagbaatar[1], B. Kindler[2], J.V. Kratz[3], J. Krier[2],Y. Kudou[4], N. Kurz[2], B. Lommel[2], S. Miyashita[5], K. Morimoto[4], K. Morita[4], Y. Nagame[5], H. Nitsche[9,10], K. Ooe[11], M. Schädel[5], J. Steiner[2], T. Sumita[4], K. Tanaka[4], A. Toyoshima[5], K. Tsukada[5], A. Türler[6,7], I. Usoltsev[6,7], Y. Wakabayashi[4], Y. Wang[8], N. Wiehl[1,3], S. Yamaki[4,12], Z. Qin[8]

[1]Helmholtz Institute Mainz, Mainz, Germany
[2]GSI Helmholtzzentrum für Schwerionenforschung, Darmstadt, Germany
[3]Johannes Gutenberg-Universität Mainz, Mainz, Germany
[4]Nishina Center for Accelerator-Based Science, RIKEN, Wako, Japan
[5]Advanced Science Research Center, JAEA, Tokai, Japan
[6]University of Bern, Bern, Switzerland
[7]Paul Scherrer Institute, Villigen, Switzerland
[8]Institute of Modern Physics; Chinese Academy of Sciences, Lanzhou, China
[9]University of California, Berkeley, U.S.A.
[10]Lawrence Berkeley National Laboratory, Berkeley, U.S.A.
[11]Niigata University, Niigata, Japan
[12]Saitama University, Saitama, Japan.

Abstract

A research program on the comparative study of the hexacarbonyl complexes of the group 6 elements Mo, W, and Sg (seaborgium, element 106) was started. The chemical behavior of these compounds was studied in isothermal chromatography and thermochromatography experiments. The main aim of these experiments is the synthesis and characterization of the chemical properties of $Sg(CO)_6$, which would represent the first organometallic compound of a superheavy element (i.e., with $Z \geq 104$). The first experiment resulted in the observation of $Sg(CO)_6$ formation.

A new approach, the study of the stability of gaseous complexes by investigating their thermal decomposition was applied for the lighter homolog Mo. The thermal stability of $Mo(CO)_6$ towards different surface materials was investigated. These studies serve as a basis for further comparative experiments with $W(CO)_6$ and $Sg(CO)_6$.

Here, preliminary results of these experiments are reported.

1. Research Objectives

In the last decades, simple inorganic compounds of the transactinide elements (TAN) were studied in gas phase chemical reactions [1]. Accessing, e.g., metal complexes with organic ligands or organometallic compounds was almost impossible due to technical restrictions, like the destructive plasma present behind the target created by the intense heavy ion beam. Thanks to the novel approach of physical preseparation in a recoil separator to reject the beam [2], these limitations could be overcome [3]. In previous experiments conducted at the TRIGA Mainz research reactor and the gas-filled recoil separator TASCA at GSI Darmstadt, we demonstrated the formation of volatile d-element carbonyl complexes with recoiling ions thermalized in a carbon monoxide containing atmosphere [4]. Short-lived isotopes of the lighter homologs of seaborgium – molybdenum and tungsten showed this to be an appropriate method to study group 6 elements under conditions relevant for a transactinide chemistry experiment. Fully relativistic quantum chemical calculations on the stability and gas chromatographic behavior of the group-6 hexacarbonyls were preformed [5], largely confirming the predicted high stability of $Sg(CO)_6$ [6, 7] which should allow its experimental observation. At the GAs-filled Recoil Ion Separator (GARIS) at RIKEN, Wako, the production and decay properties of the most suitable known isotope of element 106, ^{265}Sg, have been studied in physical preseparation experiments [8]. The presence of two isomeric states, previously inferred indirectly [9, 10], was confirmed [8]. As the ordering of the levels remains unclear, the notation ^{265a}Sg ($T_{1/2}$=8.5 s; E_α = 8.84 MeV) and ^{265b}Sg ($T_{1/2}$=14.4 s; E_α = 8.69 MeV) is generally used. Building up on these preparatory studies, the synthesis of $^{265}Sg(CO)_6$ was envisaged as a first step towards organometallic chemical studies of superheavy elements.

2. Research Contents and Results

2.1 Experiments on the gas phase chromatographic behavior of $M(CO)_6$ at RIKEN

In March 2013, an on-line experiment on the chemical investigation of the tungsten and seaborgium hexacarbonyl complexes was conducted at the GARIS Separator at RIKEN. Their formation and adsorption interaction on a SiO_2 surface was studied.

The experiment was divided into two parts. In the first part, short-lived α-decaying tungsten and radon isotopes were produced in the nuclear fusion reactions $^{144}Sm(^{24}Mg,4\text{-}5n)^{163,164}W$ and $^{nat}W(^{24}Mg,xn)^{200\text{-}204}Rn$. In the second part of the beamtime, ^{22}Ne beam was used for the production of ^{265}Sg in the reaction $^{248}Cm(^{22}Ne,5n)^{265}Sg$.

The cross-section of the reaction $^{144}Sm(^{24}Mg,4\text{-}5n)^{163,164}W$ is about seven orders of magnitude higher than the cross-section of $^{248}Cm(^{22}Ne,5n)^{265}Sg$. Tungsten as the lighter homolog of seaborgium was therefore used to optimize the experimental conditions for the studies of seaborgium. Furthermore, as both experiments were conducted under the same conditions, they allow for a direct comparison of the chemical behavior of tungsten and seaborgium.

To gain information on the chemistry-independent transport time and yield, the inert gas radon, which is volatile in elemental form, was studied as well. Any potential added delay between nuclear synthesis and the arrival time in the detection system of W and Sg compared to that of Rn can then be ascribed to the chemical reaction to form the hexacarbonyl complexes.

Initially, short-lived ^{163,164}W was produced and guided into a focal plane detector consisting of nine 28 x 28 mm^2 large PIN diodes arranged in a 3 x 3 array installed behind a honeycomb grid with 84% transmission. These measurements allowed to determine the optimum magnet setting of GARIS for the subsequent chemical experiments and to simultaneously obtain the rate at which the W nuclei were reaching the focal plane, the knowledge of which is necessary for the determination of the chemical yield in the subsequent chemistry experiments. Here they pass a grid and are implanted in the detector. A schematic of this setup is shown in Fig. 1.

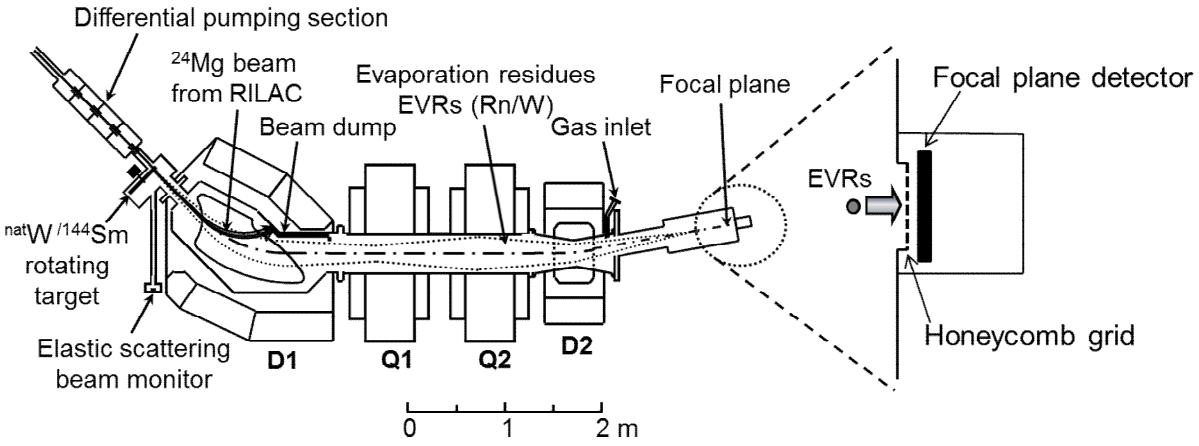

Fig. 1 Schematic drawing of the experimental setup for optimizing the magnet settings of GARIS.

A typical spectrum measured for the reaction ^{144}Sm(^{24}Mg,4-5n) in the focal plane detector is shown in Fig. 2. ^{163}W and ^{164}W can be identified by their α-decay lines. However, the highest count rate is due to the implantation of ions recoiling from the target.

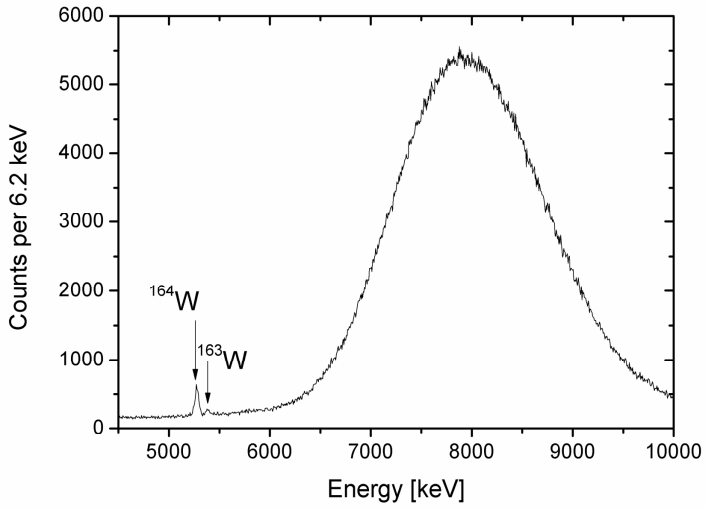

Fig. 2 Typical spectrum measured in the central diode of the focal plane detector. ^{163}W and ^{164}W can be identified by their α-decay. The main count rate originates from the implantation signals of the recoiling ions.

Subsequently, the focal plane detector was removed and a Recoil Transfer Chamber (RTC) [11, 12] was attached for the chemistry studies. The RTC contains a gas-filled volume kept at a

pressure of several hundred mbar, in which the evaporation residues were thermalized. The RTC is separated from the low-pressure environment in GARIS by a thin Mylar window, which is supported by the honeycomb grid to withstand the pressure difference. The RTC is flushed with an He/CO gas mixture, which provides the chemical agent for the in-situ formation of the hexacarbonyl complexes. Along with the rapidly flowing gas, these volatile complexes are transported within a few seconds to the gas chromatography setup through thin PFA Teflon tubes (see Fig. 3). In the experiments with α-decaying isotopes, the COMPACT on-line thermochromatography system [13] equipped with SiO_2-covered detectors was used to measure the adsorption of the complexes on this surface. Along COMPACT, a negative temperature gradient from about 22°C to temperatures well below -100°C (ranging from -109°C to -138°C, depending on the experimental settings) was applied. The gas system was a closed loop, with the gas mixture continuously circulating from the RTC to COMPACT and then cartridges filled with a drying agent to keep the water content in the gas as low as possible to prevent the formation of an ice layer inside COMPACT. From the measured distribution of α-decaying isotopes in COMPACT, the adsorption enthalpy of the complexes on SiO_2 can be extracted by means of a Monte Carlo simulation technique [14, 15].

This setup was used for studying the transport of radon, the formation and transport of $M(CO)_6$ (M=W, Sg) as well as the nuclear decay properties of the different isotopes.

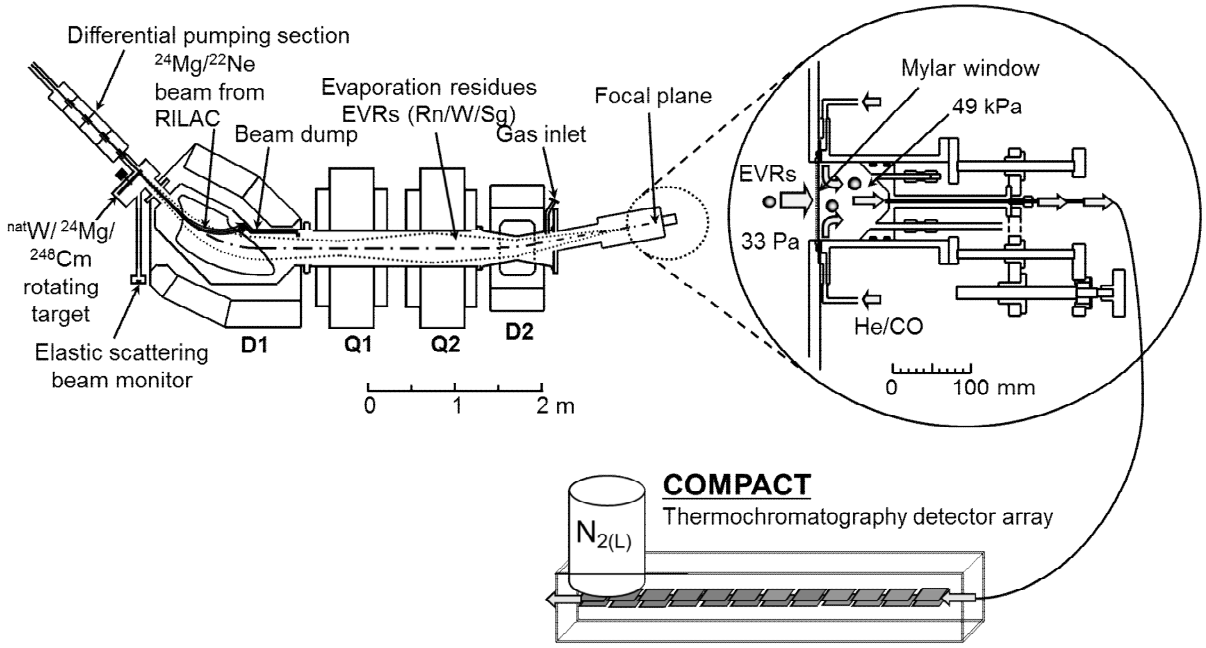

Fig. 3 Schematic drawing of the setup used for carbonyl chemistry studies. GARIS was used as a physical preseparator [11]. In the focal plane of GARIS, a recoil transfer chamber was attached. This chamber was separated from GARIS by a thin Mylar foil window. The evaporations residues pass this window and were thermalized in helium – carbon monoxide atmosphere. The volatile species were transported in the gas-stream to the thermochromatography detector COMPACT.

Figure 4 shows a typical sum spectrum of tungsten isotopes measured in the COMPACT detector array. The peak broadening is due to the fact that α particles can be emitted either into the detector, on which the compound is adsorbed, or into the one on the opposite side, implying that the α particle has to transverse the gas-filled chromatography channel, a process that leads to energy degradation.

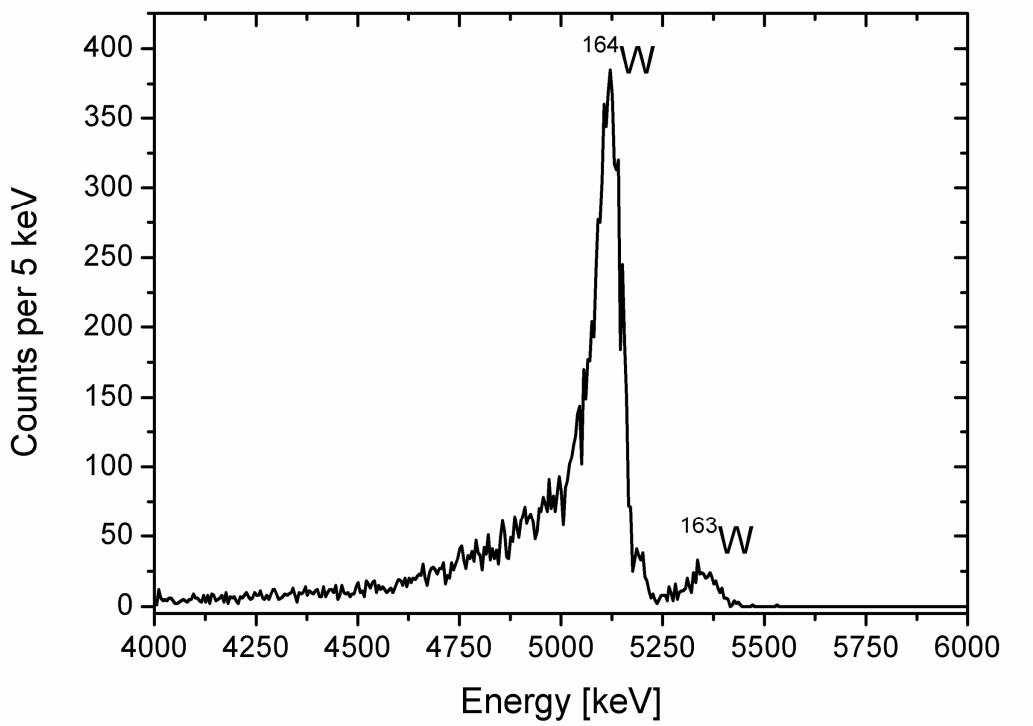

Fig. 4 Typical sum spectra of tungsten isotopes measured with COMPACT.

The extent of the peak broadening depends on the gas pressure and on the gas composition. As expected, the lower the carbon monoxide concentration, the better the obtained energy resolution.

The typical transport time for both species, elemental Rn as well as $W(CO)_6$ from the RTC to the COMPACT detector was around 5 sec depending on flow and pressure. The deposition pattern in COMPACT depends on gas flow and pressure. Fig. 5 shows a typical deposition pattern at a gas-flow rate of 1.5 L/min and a pressure of 650 mbar in the RTC.

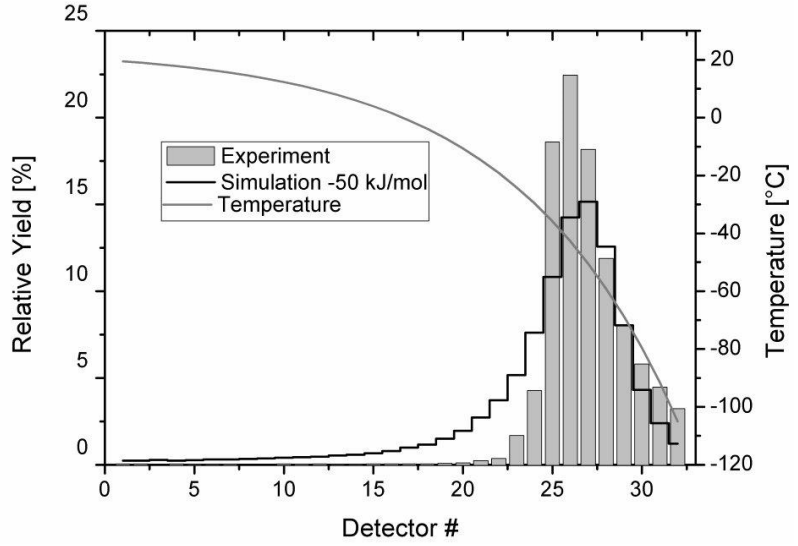

Fig. 5 Distribution of ^{163,164}W in COMPACT. The maximum of the deposition peak corresponds to a temperature of about -43 °C. All data are preliminary.

The data are in agreement with those from previous experiments [4], and the final analysis is currently under way. The tungsten experiments demonstrated the requirements for a transactinide experiment to be fulfilled, and the optimum conditions identified for tungsten served as a basis for the seaborgium studies using the ^{22}Ne(^{248}Cm,5n) reaction. Thanks to the combination of physical and chemical separation in GARIS and as seaborgium hexacarbonyl complexes, respectively, the α spectra recorded in COMPACT are extremely clean in the relevant energy region above 7.5 MeV and allow the registration of ^{265}Sg and its daughters under almost background-free conditions. As an example, we show in Fig. 6 one representative decay chain out of several observed chains, which we attribute to the decay of ^{265}Sg and its daughters, observed in the chemistry experiment in COMPACT.

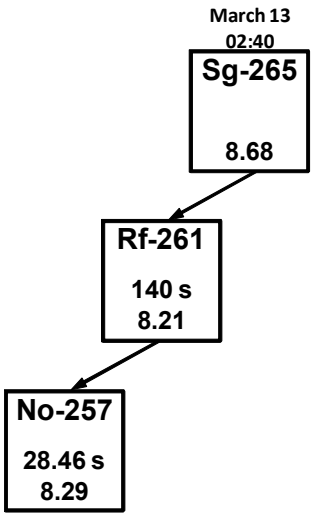

Fig. 6 One of several decay chains attributed to ^{265}Sg observed in the chemistry experiment (preliminary data).

Various experimental parameters like the gas composition and flow rate were varied to study the influence on the chemical yield. Finally, ^{265}Sg was transported from the RTC to the MANON [16] counting system with an aerosol particle gas-jet identical to that used in [8]. These data provide the rate of ^{265}Sg entering the RTC, which cannot be measured with a Si focal plane detector due to large beam-related background. The data obtained in these experiments are currently under

final analysis.

2.2. Decomposition of $Mo(CO)_6$ studied at the ^{252}Cf fission fragment source Ms. Piggy at Berne University

The successful experimental confirmation of the predicted [7] formation of seaborgium hexacarbonyl paves the way towards broader chemical studies of $Sg(CO)_6$, which may provide additional information regarding the influence of relativistic effects in the central atom of this complex. In experiments with the ^{252}Cf spontaneous fission (SF) source "Ms. Piggy" [17] installed at the University of Bern, we showed that a gas-jet system with properly chosen parameters (gas flow, decomposition surface, gas composition, etc.) is a powerful tool to study the stability of metal carbonyls. "Ms. Piggy" allows for a continuous production of different transition metal fission products with a wide variety of half-lives. Our studies focused on ^{104}Mo, ^{108}Tc, ^{109}Ru, and ^{111}Rh. Volatile metal carbonyl compounds for all these fission products form *in situ* and are transported by flushing pure CO or CO mixed with inert gas (N_2, Ar, He) through the Ms. Piggy recoil chamber at a flow rate of 1 l/min [4]. Thus, these compounds are available outside of the source for radiochemical experiments.

The carbonyl complexes were transported through a decomposition column held at variable temperatures between 25°C and 800°C. Depending on the stability of the complexes towards different surface materials kept at different temperatures, the fraction surviving the migration over this reactive section varies. The surviving complexes were trapped in a charcoal filter, which was monitored by a HPGe γ-ray detector. Thus, decomposition curves for the carbonyl complexes were obtained. The decomposition behavior of Mo carbonyl was investigated using various stationary surface materials: e.g., quartz, silver, gold, palladium, and PFA-Teflon® (Fig. 7). All metal and the quartz surface were pre-treated in CO-atmosphere at 600°C.

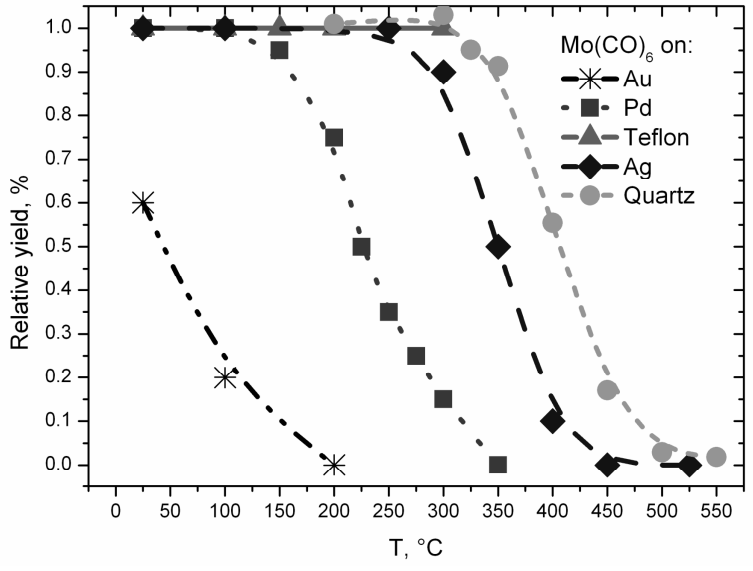

Fig. 7: Decomposition curves for ^{104}Mo carbonyl on various stationary surfaces.

The results show a clear dependence of the decomposition temperature on the used stationary surface material, suggesting that the decomposition process occurs on the surface. As follows from Fig. 6, a PFA Teflon® column cannot be used for group 6 carbonyl decomposition studies, since 100% of the carbonyls stay intact up to 300°C which is close to the melting point

of the material. 40% of ^{104}Mo carbonyl decomposes on a gold surface at ambient conditions. Of all studied elements, Mo was found to form the most stable carbonyl complexes, which decomposes only at elevated temperatures (with the exception of the gold surface). The stability differences between the various surfaces prove that the technique is appropriate for chemical investigation of the stability of group-6 metal carbonyls. Further experiments with the other seaborgium homolog, tungsten, shall reveal, which surface would be optimum to study the thermal stability trend within group 6 carbonyls, including seaborgium hexacarbonyl.

3. Conclusion

An experimental program on the study of group 6 hexacarbonyl compound was started and a first experiment on the synthesis of $Sg(CO)_6$, the first organometallic compound of a superheavy element, was performed. Its formation and interaction with a SiO_2 surface was compared to that of $W(CO)_6$. In separate experiments, the stability of $Mo(CO)_6$ was investigated.

This work was performed at the RI Beam Factory operated by RIKEN Nishina Center and CNS, University of Tokyo. We thank the ion source and accelerator staff at the RIKEN Nishina center for accelerator based research for providing intense and stable ion beams and V. Pershina for interesting discussions. The present work is partially supported by the Reimei Research Program (Japan Atomic Energy Agency), the German Federal Ministry for Education and Research, the Swiss National Science Foundation, the U.S. Department of Energy, Office of Science, Chemical Sciences, Geosciences, & Biosciences (CSGB), Division, Heavy Element Chemistry program, and the National Natural Science Foundation of China .

4. References

[1] A. Türler, and V. Pershina, Chem. Rev. **113**, 1237 (2013).
[2] Ch. E. Düllmann *et al.*, Nucl. Instrum. Methods A **551**, 528 (2005).
[3] Ch. E. Düllmann *et al.*, Radiochim. Acta **97**, 403 (2009).
[4] J. Even *et al.*, Inorg. Chem. **51**, 6431 (2012).
[5] V. Pershina, and J. Anton, J. Chem. Phys. **138**, 174301 (2013).
[6] C. S. Nash, and B. E. Bursten, New. J. Chem. **19**, 669 (1995).
[7] C. S. Nash, and B. E. Bursten, J. Am. Chem. Soc. **121**, 10830 (1999).
[8] H. Haba *et al.*, Phys. Rev. C **85**, 024611 (2012).
[9] Ch. E. Düllmann, and A. Türler, Phys. Rev. C **77**, 064320 (2008).
[10] Ch. E. Düllmann, and A. Türler, Phys. Rev. C **78**, 029901(E) (2008).
[11] H. Haba *et al.*, J. Nucl. Radiochem. Sci. **8**, 55 (2007).
[12] J. Even *et al.*, Nucl. Instrum. Methods A **638**, 157 (2011).
[13] J. Dvorak *et al.*, Phys. Rev. Lett. **97**, 242501 (2006).
[14] I. Zvara, Radiochim. Acta **38**, 95 (1985).
[15] J. Even, PhD Thesis, Johannes Gutenberg University Mainz, Germany (2011).
[16] Y. Nagame *et al.*, J. Nucl. Radiochem. Sci. **3**, 85 (2002).
[17] Ch. E. Düllmann *et al.*, Nucl. Instrum. Methods A **512**, 595 (2003).

2. Spin-orbit and Spin-lattice Coupling

Gerrit E.W. Bauer,[1] Timothy Ziman,[2] Michiyasu Mori[3]

[1]Kavli Institute of NanoScience, Delft University of Technology, Delft, The Netherlands and Institute for Materials Research & WPI-AIMR, Sendai, Japan
[2]Institut Laue Langevin and CNRS, Grenoble, France
[3]Advanced Science Research Center, JAEA, Tokai, Japan

Abstract

We pursued theoretical research on the coupling of electron spins in the condensed matter to the lattice as mediated by the spin-orbit interaction with special focus on the spin and anomalous Hall effects.

1. Research Objectives

This proposal addresses theoretically the effects that occur when condensed matter aggregates, i.e. electrically neutral many-particle systems, are subject to rotations and vibrations. The angular momentum thereby impressed on the subject is conserved, but can be redistributed over the motional degrees of freedom, thereby changing its physical properties in a controllable manner. Prominent illustrations are the provided by the Barnett, Einstein-De Haas, and Sagnac effects discovered roughly a century ago. Here we propose to have a fresh look at these effects from a modern perspective with applications to nanoscale electronic systems as well as observational astronomy. Fast rotation in the presence of strong spin-orbit interactions can generate spin currents as has been predicted in a relativistic formulation of the problem that could be observable for rotation velocities as low as 1 kHz. Magnons and phonons are interacting with each other via the magnetoelastic coupling. Both magnons and phonons are bosons that can be excited electrically [1] or thermally [2-4] in magnetic insulators by spin currents in proximity metallic contacts as indicated in Fig. 1. The effect of spin-lattice coupling on the spin Seebeck effect has been discussed first by [4]. Acoustically spin pumping has been observed by [5].

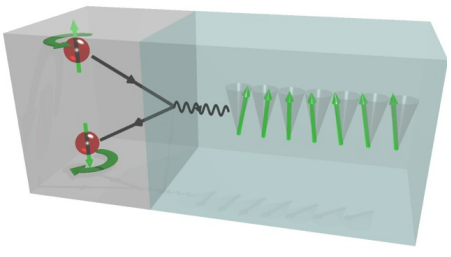

Fig. 1 The "bosonization of spintronics" rests on the magnon creation in magnetic insulators (right) by spin-polarized electron hole pairs or spinons (left).

An essential ingredient of the coupling between spin and mechanical angular momentum is the spin-orbit interaction. Materials research for strong spin-orbit interaction as is evident, e.g. in the spin Hall effect, will enhance the coupling to the lattice. The difficulty is that

spin-orbit interactions as relativistic corrections are intrinsically small except in the heaviest atoms which are less useful for practical spintronics applications. It is important, then to understand when and how these effects are enhanced and this is the common element of our investigations.

2. Research contents

We will pursue the theoretical investigation in three main directions: the role of spin-orbit coupling in phenomenological as well as microscopic calculations of the Anomalous and Spin Hall Effects, effects of spin-orbit interactions on the dynamics of a multi-ferroic oxide, and spin dependent scattering from Muonium. In each case the calculations proposed are in conjunction with a collaboration with experimentalists, at the ISSP (Kashiwa), KEK (Tsukuba), ILL (Grenoble), PSI (Zürich).

In this report we focus on the theoretical treatment of spin-orbit interactions in the solid sate, viz. the spin Hall magnetoresistance in bilayers of an insulating ferromagnet and normal metals, the AC spin Hall effect, as well as microscopic mechanisms of the Spin Hall effect including enhanced skew scattering.

3. Research results

(1) *Spin Hall magnetoresistance*

We derived a theory of a new effect called the spin Hall magnetoresistance (SMR) in bilayers made from the insulating ferromagnet F such as yttrium iron garnet (YIG) and a normal metal N with spin-orbit interaction such as platinum (Pt). The SMR is induced by the simultaneous action of spin-Hall and inverse spin-Hall effects, therefore a non-equilibrium proximity phenomenon. We compute the SMR in F|N and F|N|F layered systems, treating N by spin-diffusion theory [5] and quantum mechanical boundary conditions at the interfaces in terms of the spin-mixing conductance [6]. Our results explain the observed spin Hall magnetoresistance in N|F using reasonable values of the transport parameters [7,8]. The ferromagnet acts as an effective switchable mirror for the spin currents generated by the spin Hall effect (see Fig. 2).

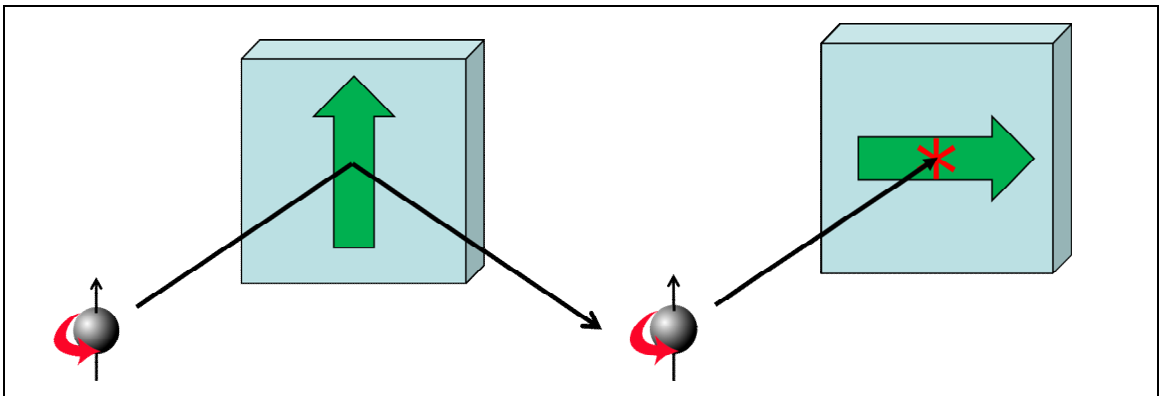

Fig. 2a Perfect spin current reflection. | Fig. 2b Efficient spin current absorption.

(2) *Spin backflow and AC spin Hall effect*

The polarization of the spin current pumped by a precessing ferromagnet into an adjacent normal metal has a constant component parallel to the precession axis and a rotating one normal to the magnetization. The former component is now routinely detected in the form of a DC voltage induced by the inverse spin Hall effect (ISHE). We computed AC-ISHE voltages much larger than the DC signals for various material combinations and discuss optimal conditions to observe the effect [9]. The backflow of spins is essential for distilling parameters from DC as well as AC spin pumping data detected by the ISHE.

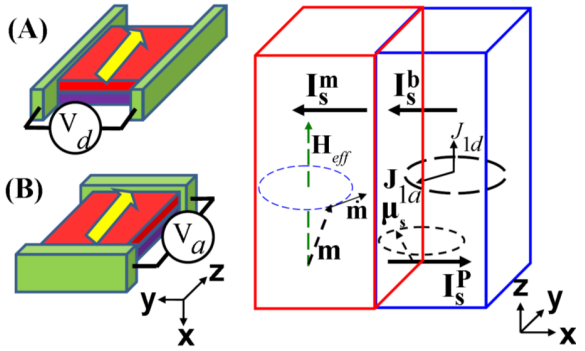

Fig. 3 Schematic spin battery operated by FMR for the measurement configurations (A) and (B). The AC(DC) voltage drops V_a (V_d) along the z(y) direction. In the right panel the magnetization **m** (time derivative precesses around the effective field H_{eff} in the left layer, generating DC/ AC spin currents and a spin accumulation in the normal metal (right side) [9].

(3) *Anomalous and spin-Hall effects from microscopic spin-orbit coupling*.

Important macroscopic manifestations of the spin-orbit coupling in solids are seen in the anomalous and spin-Hall effects. These effects are useful both for applications in novel spintronics devices and as a means of probing the microscopic spin-orbit interactions in the laboratory. Since spin-orbit effects are relativistic corrections and therefore intrinsically weak in lighter atoms, it is important to find ways of enhance their effects. Several groups [10] have now developed ways of calculating the contribution of the curvature of the Fermi surfaces in metals to the Anomalous Hall resistance. At finite temperatures such calculations can include renormalization of the band structure via a temperature-dependent shift in the shapes and positions of different bands. This neglects, however, the contribution of magnetic fluctuations, which become increasingly significant as we approach the Curie temperature. The understanding of their effects had essentially not advanced since the classic calculations of Kondo in the early 60's [11] to estimate the fluctuation-induced contribution to the Anomalous Hall coefficient. We [12] re-examined the question and showed that the work has to be extended significantly to fully account for new data

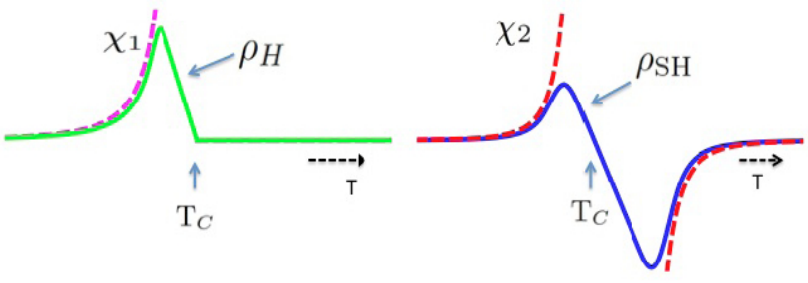

Fig. 4 Schematic form of the Anomalous and Spin Hall Effects close to the Curie temperature. In each case the transport should show an anomaly corresponding to a cut-off of the non-linear susceptibility.

from the group of Otani (ISSP, Tokyo) [13], in particular of the inverse Spin Hall Effect. Even for the Anomalous Hall Effect there are extensions to the classic Kondo calculation, which may be necessary to account for new and more accurate measurements, for example by Jin (Fudan University, Shanghai) on Ni and Ni alloys [14]. In the work of Kondo, the local moments fluctuate and, via the spin-orbit coupling, this leads to skew scattering. He included purely local fluctuations with the thermodynamics calculated within molecular field theory. In fact for metallic Ni, for example, the anisotropy is rather weak so that even at low temperatures a significant number of spin flips should occur. Such excitations, classified as "extrinsic" in the sense that the transverse coefficients will have a linear dependence on the longitudinal resistance, but "intrinsic" in the sense that these are properties of perfectly pure and crystalline materials, will be strongest in the vicinity of the Curie temperature. We extended Kondo's theory of spin-dependent skew scattering coefficients to include critical fluctuations beyond mean field theory. These included Monte Carlo estimates of the higher order spin correlations for Heisenberg spins that enter the generalized expressions for the transport coefficients that we have derived.

(4) *Spin dependent scattering from Muonium:*

Recent experiments by the group of K. Nagamine (KEK) and E. Torikai (Yamanashi) at J-Parc have raised the issue of calculating spin-dependent scattering from bound states of the Muonium$^-$ ions formed in doped GaAs by the capture of conduction electrons by positive muons. The theoretical challenge was to make quantitative estimates of both the spin-dependent scattering of conduction electrons via the spin-orbit interaction and the scattering potential of the bound ion and the spin-flip rate of the positive muon at the center of the Muonium "ion", which is coupled via the hyperfine interaction to the electrons. Estimates of the spin-dependence of the doubly-charged Mu$^-$ ion gave times too long to explain the experimental results. A new approach has been taken in which valence fluctuations can introduce a new time scale intermediate between the very rapid spin depolarization and the lifetime of the muon. We have estimated this by ab-initio estimates of the mixing of different charge states due to overlap of the bound muonium states and the GaAs host band.

4. Conclusion

The first part of the Reimei project successfully addressed various aspect of the theory of spin orbit interactions in metallic normal and ferromagnetic metals, as well as heterostructures involving ferromagnetic insulators. We may conclude that we increased the grasp on important phenomena induces by the spin orbit interactions, such as the spin Hall and anomalous Hall effects in various circumstances, as well as the Muonium physics in semiconductors. By implication, we can compute the forces and torques that the electrons exert on the lattice via the same spin orbit interaction. Next to continuation of the present line of research we will focus attention to the mechanical effects in the second part of our Reimei project.

5. Acknowledgement

We acknowledge the support of the JAEA through the Reimei program and thank the Advanced Science Research Center for hosting foreign visitors and organization of the Reimei Meetings in Tokai.

6. References

[1] Y. Kajiwara, K. Harii, S. Takahashi, J. Ohe, K. Uchida, M. Mizuguchi, H. Umezawa, H. Kawai, K. Ando, K. Takanashi, S. Maekawa, and E. Saitoh,, Nature 464, 262-266 (2010).

[2] K. Uchida, H. Adachi, T. An, T. Ota, M. Toda, B. Hillebrands, Maekawa S, Saitoh E, Nat. Mater. 10, 737 (2011).

[3] J. Xiao, G.E.W. Bauer, K. Uchida, E. Saitoh, S. Maekawa, Physical Review B 81, 214418 (2010).

[4] H. Adachi, K. Uchida, E. Saitoh, J. Ohe, S. Takahashi, and S. Maekawa, Appl. Phys. Lett. 97, 252506 (2010).

[5] S. Takahashi, H. Imamura, and S. Maekawa, in Concepts in Spin Electronics, edited by S. Maekawa (Oxford University Press, UK, 2006), pp. 343–370.

[6] A. Brataas, Yu. V. Nazarov, and G. E. W. Bauer, Phys. Rev. Lett. 84, 2481 (2000).

[7] H. Nakayama, M. Althammer, Y.-T. Chen, K. Uchida, Y. Kajiwara, D. Kikuchi, T. Ohtani, S. Geprägs, M. Opel, S. Takahashi, R. Gross, G. E. W. Bauer, S. T. B. Gönnenwein, and E. Saitoh, Phys. Rev. Lett. **110**, 206601 (2013)

[8] Y.T. Chen, S Takahashi, H Nakayama, M Althammer, S.T.B. Gönnenwein, E. Saitoh, and G.E.W. Bauer, Phys. Rev. B **87**, 144411 (2013)

[9] H. Jiao and G.E.W. Bauer, Phys. Rev. Lett. **110**, 217602 (2013).

[10] N. Nagaosa, J. Sinova, S. Onoda, A. H. MacDonald, and N. P. Ong, *Anomalous Hall Effect*, Rev. Mod. Phys. **82**, 1539 (2010).

[11] J. Kondo, *Anomalous Hall Effect and Magnetoresistance of Ferromagnetic Metals*, Prog. Theor. Phys. **27**, 772-792 (1962).

[12] B. Gu, T. Ziman, and S. Maekawa, *Theory of the Spin Hall effect in a ferromagnetic metal near the Curie temperature*, Phys. Rev. 86, 241303 (R) (2013).

[13] D. Wei , B. Gu , T. Ziman , S. Maekawa , Y. Otani, *The spin Hall effect as a probe of nonlinear spin fluctuations*, Nature Comm. 3, 1038 (2012).

[14] L. Ye, Y. Tian, X. Jin, D. Xiao, Temperature dependence of the intrinsic anomalous Hall effect in nickel, Phys. Rev. B 85, 220403(R) (2012).

3. 異方的な磁気ゆらぎで探るアクチノイド化合物の重い電子系超伝導

Heavy Fermion Superconductivity Explored by the Anisotropic Magnetic Fluctuations in Actinide Compounds

青木大[1,2]、神戸振作[3]、ジャック・フルケ[2]
Dai Aoki[1,2], Shinsaku Kambe[2], Jacques Flouquet[2]

[1]東北大学金属材料研究所
IMR, Tohoku University
[2]INAC/SPSMS, CEA-Grenoble
[3]日本原子力研究開発機構 先端基礎研究センター
Advanced Science Research Center, Japan Atomic Energy Agency

概要

強磁性と超伝導の共存や磁場誘起超伝導など、アクチノイド化合物は物性物理の宝庫である。強磁性超伝導体はイジング性のきわめて強い磁気ゆらぎが発達し、超伝導上部臨界磁場がきわめて高い特異な超伝導相図を示す。一方、銅酸化物超伝導体や Ce115 系など、XY 型の横の磁気ゆらぎが発達して高い超伝導転移が実現している場合もある。本研究では、純良単結晶を用いた異方的な磁気ゆらぎに着目した研究を行ない、多数の成果を得ることができた。

1. 研究目的

アクチノイド化合物の物性をになう 5f 電子は、局在（4f 電子）と遍歴（d 電子）の中間的な性質を持ち、さらにスピンと軌道の自由度を持つ。このため強磁性と超伝導の共存[1]、「高温」超伝導、隠れた秩序、多極子秩序など多彩な物理を展開する。これまで、30 を越える重い電子系超伝導体が発見されているが、このうち 10 以上の物質がアクチノイド化合物である。アクチノイド化合物は物性物理の宝庫であり、いまだ未踏の領域である。しかし、放射性物質取り扱いの規制の強化により、現在アクチノイド化合物の試料育成と精密物性測定ができる施設は世界でも限られている。

本研究の目的はまず（1）アクチノイド化合物における新物質開発と新奇超伝導体の探索、そして（2）縦の磁気ゆらぎによる高い超伝導臨界磁場、横の磁気ゆらぎによる高い超伝導転移温度の発現機構の微視的測定手段による解明、およびその指針に基づいた物質開発である。

物性物理において新物質は研究の生命線である。本研究では、アクチノイド化合物に焦点を絞り、新たな強磁性超伝導物質、磁気量子臨界点近傍物質を探索する。希土類化合物に比べて、アクチノイド化合物の既知の物質は少なく、しかも純良単結晶による極低温までの実験報告例はきわめて限られている。エネルギー問題が重要な課題となる中、優れた特性を持つ新たな超伝導物質の探索は、応用面からきわめて重要である。そのためには、新物質開発とともに高い超伝導転移温度、高い臨界磁場の発現機構を基礎研究の立場から解明することは重要な意味を持つ。とくに、アクチノイド化合物は比較的純良な試料が得られるために、温度、磁場、圧力などの外部パラメータで物質を磁気不安定点近傍にチューニングして精密測定を行う上で格好の舞台となる。このような視点からア

クチノイド研究が行われた例はあまりなく、しかも実際に出来る施設は限られている。本研究は、原子力機構先端研、東北大金研大洗センターを研究拠点とし、国際的な研究協力としてフランス原子力庁 CEA-Grenoble も本研究課題に参画した。

2. 研究内容

当初、予定していた研究計画は以下の通りである。（1）アクチノイド化合物における新物質開発と純良単結晶育成、（2）ウラン強磁性超伝導体の磁場誘起超伝導の発現機構の解明、（3）XY 型ゆらぎによる超伝導発現機構と超伝導転移温度の解明、である。

（1）アクチノイド化合物における新物質開発と純良単結晶育成

アクチノイド化合物は、5f 電子が局在して大きな磁気モーメントを持つ物質から、遍歴して常磁性になっている物質まできわめてバラエティに富んでいる。このうち物理的に興味深いのは、磁気秩序寸前の物質あるいは、弱い磁気秩序を示す物質である。希土類化合物では圧力などの外部パラメータによって臨界点にチューニングする。これに対してアクチノイド化合物は、すでに臨界点にチューニングされている場合が多く常圧でさまざまな精密測定手段が可能である。新物質開発の指針として、i)異方的な磁気ゆらぎ（高イジング->高 H_{c2}, 高 XY->高 T_c）ii)層状、カゴ状、ジグザグチェーンなど特徴的な結晶構造、iii)小さな磁気モーメント、iv)大きな電子比熱係数、に注目し、テトラアーク炉、フラックス炉、ブリッジマン炉、気相成長炉、高周波炉などの多様な試料育成装置を駆使して行う。単結晶育成を効率的に行うための装置の整備も行う。育成された試料は、組成の確認、結晶構造の決定が重要である。そのために EPMA、X 線単結晶構造解析による試料の同定を行う。さらに、得られた試料について、極低温までの電気抵抗測定・磁化測定による試料評価を詳細に行う。

（2）ウラン強磁性超伝導体の磁場誘起超伝導の発現機構の解明

強磁性と超伝導が微視的に共存する系はウラン化合物 UGe_2、URhGe、UCoGe の三種類である。いずれの物質も超伝導転移温度は 1K 以下と低いにもかかわらず、通常の BCS 型超伝導から期待される値より数十倍も高い上部臨界磁場 H_{c2} を持つ。さらに、いずれの物質も磁場再突入（リエントラント）型の H_{c2} 相図を示す。電気抵抗、比熱、磁化測定などのマクロ測定から、強磁性の縦の磁気ゆらぎによって増強されたスピン三重項の平行スピン対が超伝導を担っていると考えられる。本研究では、NMR、量子振動によるフェルミ面の観測、中性子散乱実験などの微視的測定手段から超伝導発現機構の解明に迫る。とくに、T_1 の測定によるスピンゆらぎの異方性、フェルミ面の直接観測による対称性の破れとトポロジーによる新量子相、磁気励起と異方的超伝導ギャップの形成などについて注目する。

（3）XY 型ゆらぎによる超伝導発現機構と超伝導転移温度の解明

アクチノイド化合物とくに超ウラン化合物の超伝導転移温度は高く、重い電子系超伝導（Ce の 4f 電子系）と銅酸化物高温超伝導（d 電子系）の間をつなぐものと考えられている。超伝導体の統一的理解のためにアクチノイド化合物超伝導は重要な位置を占めている。反強磁性の XY 型の横ゆらぎが超伝導転移温度と関係しており、これを NMR などの微視的測定手段により解明する。また、得られた知見を指針として新たな「高温」超伝導体を探索する。NMR 測定装置は上述の先端研所有、金研設置済みの装置を利用する。必要に応じて、ILL での非弾性

中性子散乱実験、大型放射光施設 ESRF や SPring8 での共鳴 X 線散乱実験も行なう。

3. 研究結果

このうち、（1）については、カゴ状やジグザグチェーン、反転対称性がないなど特徴的な結晶構造に着目して物質開発を行なった。また、大きな電子比熱係数、低い磁気秩序温度、適度なウラン原子間の距離などにも着目して様々な試料を、引き上げ法、フラックス法、ブリッジマン法などの方法で育成した。得られた試料は、手製の ADR（断熱消磁冷凍）セルを用いて、100mK までの電気抵抗測定をセッティングから測定終了まで数時間で済ませるなど、迅速な試料評価を大量の試料に対して行なった。その結果、強磁性超伝導体 UCoGe においては、残留抵抗比が 200 を越える世界最高純度の単結晶育成に成功した。また、「隠れた秩序」を持つ URu_2Si_2 においては、残留抵抗比 500 を越える超純良単結晶育成に CEA-Grenoble、原子力機構先端研の両研究所で成功し、試料は多方面に提供されている。なお、URu_2Si_2 の試料育成と評価については JPSJ に発表され[2]、「Papers of Editors' Choice」、「2012 Highly Cited Article」に選ばれている。

（2）については、引き上げ法によって得られた高純度強磁性超伝導体 UCoGe、URhGe、UGe_2 に焦点をあて、電気抵抗測定、磁場中比熱、AC 帯磁率、熱電能、熱伝導度、ドハース・ファンアルフェン（dHvA）効果、シュブニコフ・ドハース（SdH）効果、パルス強磁場による磁化、電気抵抗測定などさまざまな実験を行なった。その結果、URhGe、UCoGe においては、SdH 効果によって小さなポケットフェルミ面の観測に成功した[3,4]。とくに UCoGe の観測されたフェルミ面はメタ磁性とともに dHvA 振動数の分裂が観測された。磁場による有効質量の増大とフェルミ面の不安定性、さらには、磁場によって安定化する超伝導相との関連を現在詳細に調べているところである。さらに、強磁性の臨界圧力 P_c 以上でもフェルミ面が観測されており、フェルミ面と強磁性超伝導の関係を調べる上で、今後重要なテーマになると考えられる。

UGe_2 については、磁場 Sweep 中の熱電能測定による量子振動現象の観測に成功した[5]。これは、我々の知る限り重い電子系アクチノイド化合物で得られた初の熱電能量子振動測定である。振動数

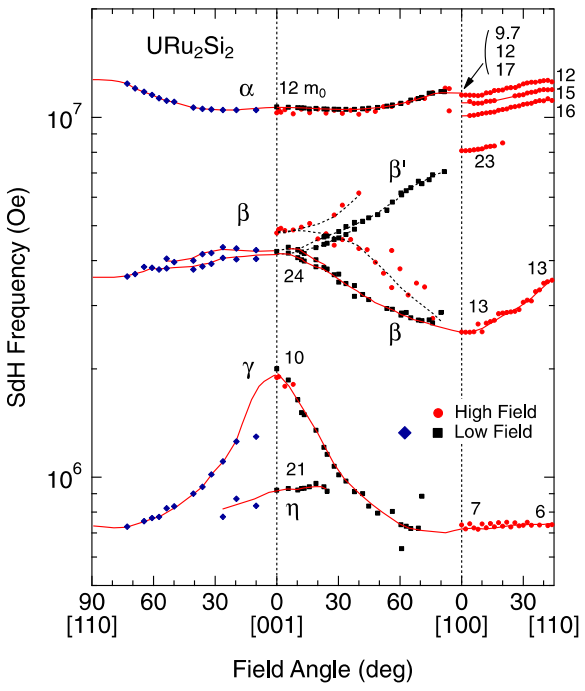

図 1: URu_2Si_2 の dHvA 振動数の角度依存性[6]

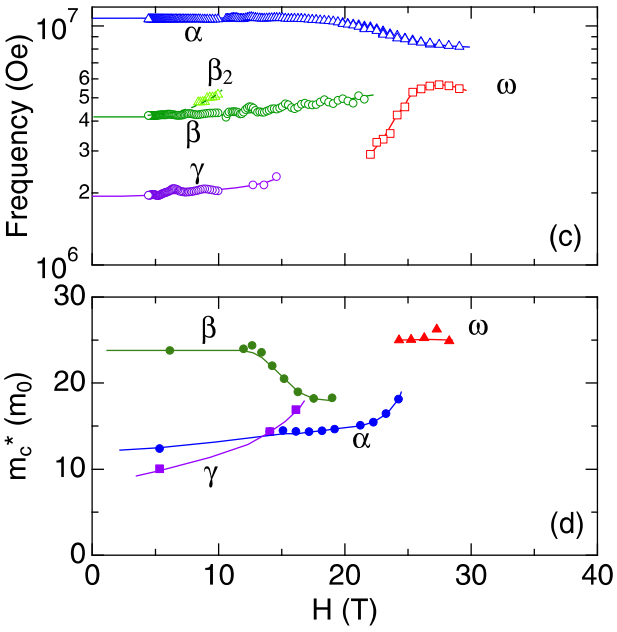

図 2: URu_2Si_2 の dHvA 振動数、サイクロトロン有効質量の磁場依存性[6]

は過去の dHvA 効果と良く一致しており、熱電能測定においても信頼性の高いフェルミ面観測が出来ていることを示している。

また、URu_2Si_2については、dHvA 効果、および強磁場 SdH 効果によってフェルミ面のほぼ全容が明らかになった[6]。図 1 に示すように、α、β、γブランチを全磁場角度領域で観測し、フェルミ面の形状とブリルアンゾーンにおける位置を明らかにした。しかしながら、比熱係数を説明するためには、観測されていない重いフェルミ面がもう一つ存在するはずである。「隠れた秩序」の臨界磁場（H_c~35T）近傍では、フェルミ面の体積、有効質量の大きな変化、新しいフェルミ面の出現が観測された（図 2 参照）。低キャリアで重い準粒子を伴うURu_2Si_2のフェルミ面は、磁場によるゼーマン効果によって影響を受けやすい。磁場による「隠れた秩序」の抑制は、磁場によるフェルミ面の不安定性およびギャップエネルギーE_0と E_1の磁場応答と直接関連していると考えられる。強磁場下におけるフェルミ面の再構築は強磁場熱電能、ネルンスト効果測定によっても確認された[7]。

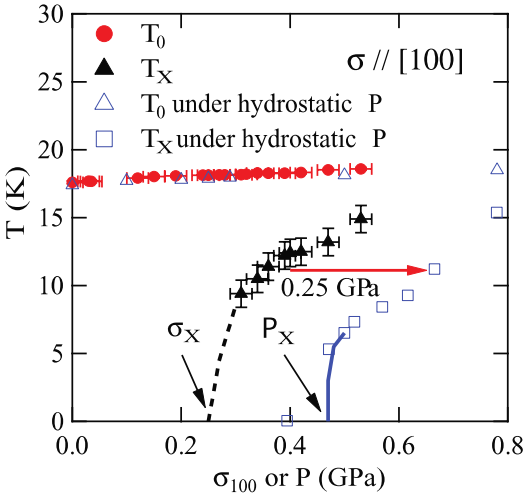

図 3: URu_2Si_2の一軸圧力下の温度・圧力相図[8]

URu_2Si_2 の一軸圧力下の熱膨張測定も行なった[8]。その結果、図 3 に示すように、正方晶の[100]方向に一軸圧力を加えると、静水圧の場合よりも低い圧力で「隠れた秩序」抑制されて反強磁性が現れることがわかった。一方、[110]方向の一軸圧力では、0.6GPa まで反強磁性は現れない。これは c 面内のウラン間の距離によって、臨界圧が決まっていることを示唆している。

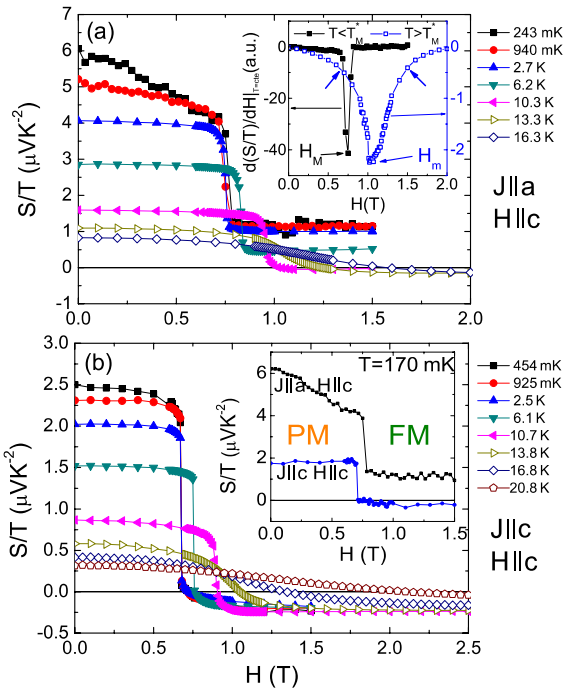

図 4: UCoAl のさまざまな温度における熱電能の磁場依存性[9]

（3）については、まず、強磁性量子臨界点近傍にある UCoAl に焦点をあてて研究を行なった。この物質は、結晶構造に反転対称性が無い擬カゴメ格子を形成している。磁気ゆらぎがきわめて異方的であり、Ising 性の強いゆらぎを持っている。このため、常圧で磁場を加えると常磁性から強磁性へとメタ磁性転移を示す。圧力を加えるとメタ磁性転移は高磁場へとシフトして行き、1.5GPa、7T でメタ磁性の一次転移が消失し、ブロードなクロスオーバーとなる。すなわち強磁性量子臨界終点を迎える。常圧下の極低温熱電能測定により、このメタ磁性を詳細に調べた。その結果、図 4 に示すように、メタ磁性による一次相転移が明瞭に観測された。興味深いのは熱流の方向（J//a 軸, J//c 軸）により振る舞いが大きく異なることである。フェルミ面は多バンドにより形成され、重い準粒子を持つホール面がメ

タ磁性によって大きく変化していることが分かった。

4. まとめ

重い電子系ウラン化合物のさまざまな物質において、純良単結晶育成をおこない、極低温の物性測定を行なった。歴史的には純良単結晶育成と物質開発はこの分野における要の一つであり、研究のフロンティアを切り開いて来た。本研究では、きわめて純良なウラン化合物の単結晶を育成することにより、上に説明したような多数の成果が得られた。今後、強磁場 NMR や一軸圧 NMR/NQR など極限環境下における微視的物性測定をさらに進展させたい。

5. 参考文献

[1] D. Aoki and J. Flouquet: J. Phys. Soc. Jpn. 81(2012) 011003.
[2] T.D. Matsuda, E. Hassinger, D. Aoki, V. Taufour, G. Knebel, N. Tateiwa, E. Yamamoto, Y. Haga, Y. Ōnuki, Z. Fisk and J. Flouquet: J. Phys. Soc. Jpn. **80** (2011) 114710.
[3] D. Aoki et al.: in press.
[4] G. Knebel et al.: in press.
[5] A. Pourret et al.: in press.
[6] D. Aoki, G. Knebel, I. Sheikin, E. Hassinger, L. Malone, T.D. Matsuda, J. Flouquet: J. Phys. Soc. Jpn.81 (2012) 074715.
[7] A. Pourret, A. Palacio-Morales, S. Krämer, L. Malone, M. Nardone, D. Aoki, G. Knebel and J. Flouquet:J. Phys. Soc. Jpn. **82** (2013) 034706.
[8] S. Kambe, D. Aoki, B. Salce, F. Bourdarot, D. Braithwaite, J. Flouquet, and J.-P. Brison: Phys. Rev. B **87**, (2013) 115123
[9] A. Palacio-Morales,1, A. Pourret, G. Knebel, T. Combier, D. Aoki, H. Harima, J. Flouquet: Phys. Rev. Lett.110 (2013)116404.

4. Synthesis and Characterization of Novel Diluted Ferromagnets Istostructural to the 111, 122 and 1111 FeAs Superconductors

K. Zhao[1], Z. Deng[1], X. C. Wang[1], W. Han[1], J. L. Zhu[1], X. Li[1], Q.Q. Liu[1], R.C. Yu[1], T. Goko[2], B. Frandsen[2], Lian Liu[2], Fanlong Ning[2,3], C. Ding[3], Y.J. Uemura[2], H. Dabkowska[4], G.M. Luke[4], H. Luetkens[5], E. Morenzoni[5], S.R. Dunsiger[6], A. Senyshyn[6], P. Böni[6], W. Higemoto[7], T. Ito[7], Bo Gu[7], S. Maekawa[7], and C.Q. Jin[1]

1) *Beijing National Laboratory for Condensed Matter Physics, and Institute of Physics, Chinese Academy of Sciences, Beijing 100190, China*
2) *Department of Physics, Columbia University, New York, New York 10027, USA*
3) *Department of Physics, Zhejiang University, Hangzhou 310027, China*
4) *Department of Physics and Astronomy, McMaster University, Hamilton, Ontario L8S 4M1, Canada*
5) *Paul Scherrer Institute, Laboratory for Muon Spin Spectroscopy, CH-5232 Villigen PSI, Switzerland*
6) *Physics Department and FRM-II, Technische Universität München, D-85748 Garching. München, Germany*
7) *Advanced Science Reserch Center, Japan Atomic Energy Agency, Tokai 319-1195, Japan*

Abstract:

We report synthesis, characterization, and theoretical calculations of novel diluted ferromagnets Li(Zn,Mn)As, (Ba,K)(Zn,Mn)$_2$As$_2$, and (La,Ba)(Zn,Mn)AsO, having similar or identical crystal structures with those of the "111", "122," and "1111" FeAs superconductors, with a very good matching of lattice constants. The isovalent (Zn,Mn) substitutions allow synthesis of bulk specimens, with the ferromagnetic Curie temperatures up to about 200 K. These systems may be useful for future development of spin sensitive electronics devices with junctions and multi-layers composed of combinations of these ferromagnets, FeAs superconductors, iso-structural antiferromagnets (with 100% Mn) and semiconductors (with 100% Zn). Here we review three years of our effort supported by the Reimei Research Funding from JAEA.

1. Introduction / Research Objectives

Studies of diluted magnetic semiconductor (DMS) systems developed with synthesis and characterization of a prototypical system (Ga,Mn)As based on a III-V semiconductor GaAs. In

this system, substitution of trivalent Ga^{3+} with divalent Mn^{2+} results in severely limited solubility, and specimens are available only as thin films generated by Molecular Beam Epitaxy (MBE) methods [1].

This feature also leads to high sensitivity of materials qualities to heat treatments and inhomogeneous properties reported for less-optimized specimens. The spin doping with the (Ga,Mn) substitution results in simultaneous hole charge doping, restricting the system to be always p-type semiconductors. Twenty years of effort in raising the ferromagnetic T_C have led to the current limit of T_C up to about 200 K in (Ga,Mn)As [1-3]. In 2007, Jungwirth and co-workers [4] proposed to replace trivalent Ga with divalent Zn plus monovalent Li, and dope Mn into the isovalent Zn sites, while controlling charge concentrations with excess or deficient Li concentrations. Following this suggestion, and aiming to synthesize new DMS systems available with bulk specimens in both p- and n-type doping, we have generated novel DMS systems with (Zn,Mn) substitutions on I-II-V semiconductor LiZnAs, as well as relevant semiconductors $BaZn_2As_2$ and LaZnAsO. These ferromagnetic DMS systems have been characterized by transport, magnetic, structural, MuSR, and NMR measurements.

2. Research Contents

In the beginning of 2010, one of the authors (YJU) attended a conference held in Sendai for spintronics materials to report MuSR results on conventional DMS material (Ga,Mn)As [5], and learned about the theoretical proposal [4] to generate Li(Zn,Mn)As in a presentation made by Thomas Jungwirth. There was no attempt to synthesize this system, however, made by members of traditional DMS research community due to difficulties of handling Li and multiple elements in MBE materials growth. Based on experiences accumulated in materials growth of LiFeAs [6] and other FeAs superconductors, we decided to challenge synthesis of this system as bulk specimen at IOP in Beijing. Within two months, we succeeded in synthesizing Li(Zn,Mn)As which exhibits ferromagnetic order with the Curie temperature T_C up to ~ 50 K, and characterized the material by structural analyses using x-ray scattering, transport measurements including Hall effect, magnetization measurements including observation of the hysteresis loop, and muon spin relaxation studies. In order to explain un-expected p-type carrier doping in the case of materials with excess Li concentrations, theoretical calculations were made to compare energy stability of a few different candidate site locations of excess Li. These results were published in a Nature Communications paper in 2011 [7],

Within two years after this initial effort, we were able to synthesize a similar system $(Ba,K)(Zn,Mn)_2As_2$, with T_C up to ~ 200 K, having the crystal structure identical to that of a high-Tc superconductor $(Ba,K)Fe_2As_2$. This system was characterized by using x-ray and neutron scattering measurements for structural analyses, standard transport and magnetic measurements, and muon spin relaxation measurements to confirm homogeneity of magnetic order over the entire volume of the material. The synthesis of this novel DMS system was reported in another paper published in Nature Communications in 2013 [8]. In the case of (Ga,Mn)As, more than 10 years of accumulated effort was required to obtain materials having T_C ~ 200 K. In view of this, the synthesis of the new DMS materials based on the “122”

structure is a remarkable achievement. Further efforts on materials developments and optimizing heat treatment may allow raising T_C to even higher temperatures close to room temperature.

Very recently, we also succeeded in synthesizing another new DMS system (La,Ba)(Zn,Mn)AsO, with T_C up to ~ 30 K [9], which have a crystal structure identical to that of the "1111" superconductor LaFeAs(O,F). This achievement indicates that most of the FeAs-based superconductors may have their companion DMS system generated by replacing Fe with (Zn,Mn) atoms. In addition to As compounds we already found that Li(Cd,Mn)P becomes ferromagnetic [10]. There will be a large number of DMS ferromagnets composed of transitional metals different from Mn and As atom replaced by P, Sb, and some other elements.

3. Research Results:

3-1: Magnetic properties

Results of the magnetization measured in the field cooling (FC), zero-field cooling (ZFC) and isothermal field cyclic hysteresis procedures are shown for the "111" DMS Li(Zn,Mn)As in Figure 1(a)-(b), and for the "122" DMS $(Ba,K)(Zn,Mn)_2As_2$ in Figure 2(a)-(b).

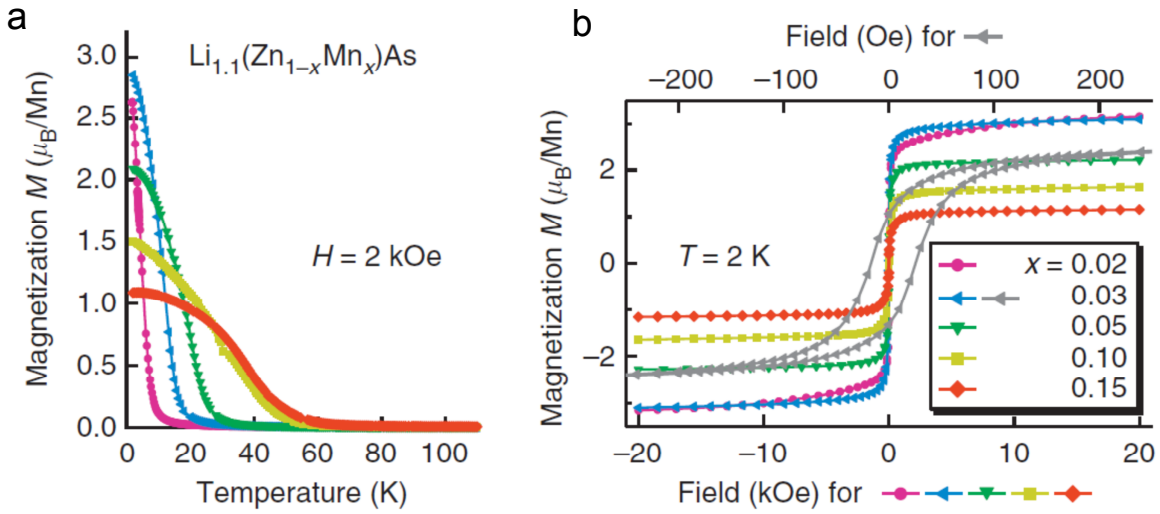

Fig. 1: The magnetization of $Li_{1.1}(Zn_{1-x},Mn_x)As$ obtained in the external field of 2 kG in field cooling (a; left) and in the isothermal field cycling at T= 2 K (b; right). The coercive field is only about 50 G, as shown by the gray symbols in (b). [7] (see [7] for color figures)

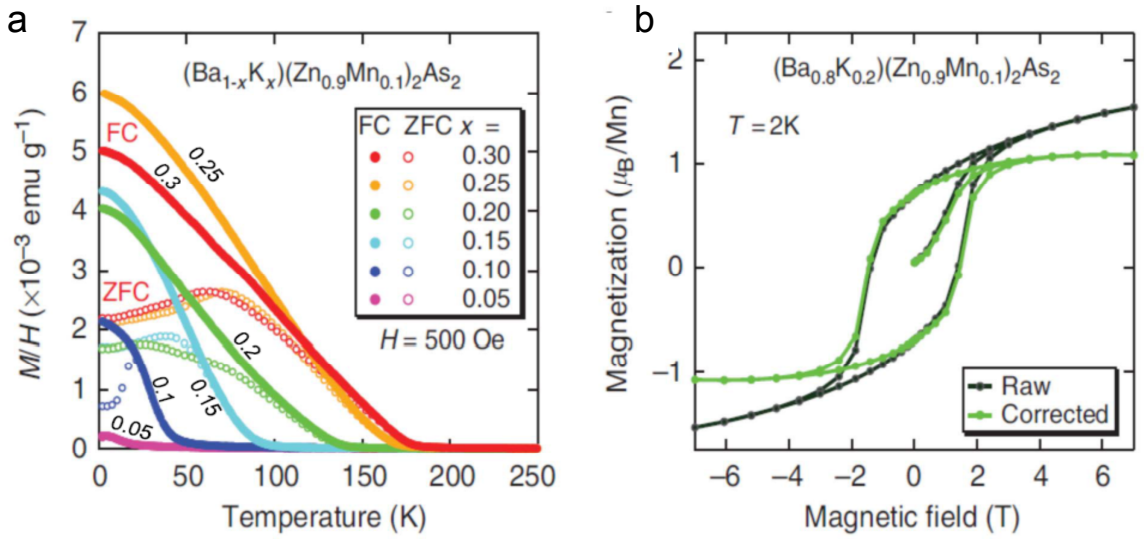

Fig. 2: The magnetization of $(Ba_{1-x}K_x)(Zn_{0.9}Mn_{0.1})_2As_2$ obtained in the external field of 500 G in field cooling and zero field cooling for various charge doping levels x (a; left) and in the isothermal field cycling at T= 2 K for x =0.2 (b; right). [8] (see [8] for color figures)

As shown in Figures 1 and 2, the saturation moment is 1-2 Bohr magnetons per Mn in both the 111 and 122 DMS systems, indicating strong ferromagnetic spin correlations. The Curie temperature is nearly 200 K in the 122 system. A pronounced irreversibility of magnetization and a large coercive field is seen in the case of the 122 systems, suggesting large anisotropy. Very recently, we also generated the 1111 DMS system (La,Ba)(Zn,Mn)AsO [9] having T_C up to ~ 40 K, which exhibits irreversibility and coercive field comparable to those of the 122 DMS systems.

3-2: Charge transport and sign of carriers

Parent compounds of these systems without spin and charge dopings, LiZnAs, $BaZn_2As_2$ and LaZnAsO, are direct-gap semiconductors. In the 111 DMS system, both excess and deficiency of Li concentrations from the stoichiometry lead to metallic charge conduction [7]. Ferromagnetic 111 DMS compounds can be obtained only for the case of Li excess, which nominally implies n-type electron doping. Contrary to this naïve expectation, the Hall effect measurements revealed p-type carriers in Li excess 111 DMS systems [7], which presumably results from excess Li occupying Zn site, acting as an accepter. This hypothesis was supported by chemical analyses and theoretical calculations using LDA and quantum Monte Carlo methods [6].

The (Ba,K) substitution in the 122 DMS and the (La,Ba) substitutions in the 1111 DMS systems both result in doping holes, as confirmed by the Hall effect measurements [8,9]. Thus,

all the three novel DMS systems have p-type hole carriers. The resistivity of the spin and charge doped 122 and 1111 DMS systems exhibit a mild semiconducting behavior, suggesting achievements of ferromagnetic coupling of spins by charge carriers without full delocalization. Similar situation has been noticed in (Ga,Mn)As with small Mn concentrations [5]. These features demonstrate that ferromagnetic network can be supported with charge carriers having limited range of spatial spread.

3-3: MuSR measurements

We performed MuSR measurements on conventional DMS system (Ga,Mn)As at Paul Scherrer Institute (PSI) [5] using MBE film specimens, and in all these novel 111, 122,and 1111 DMS systems at TRIUMF (Vancouver) and PSI (Zurich) using bulk poly-crystalline specimens [7-9]. Figure 3(a)-(c) show the time spectra of Zero-Field MuSR observed in the 111,122, and 1111 DMS systems.

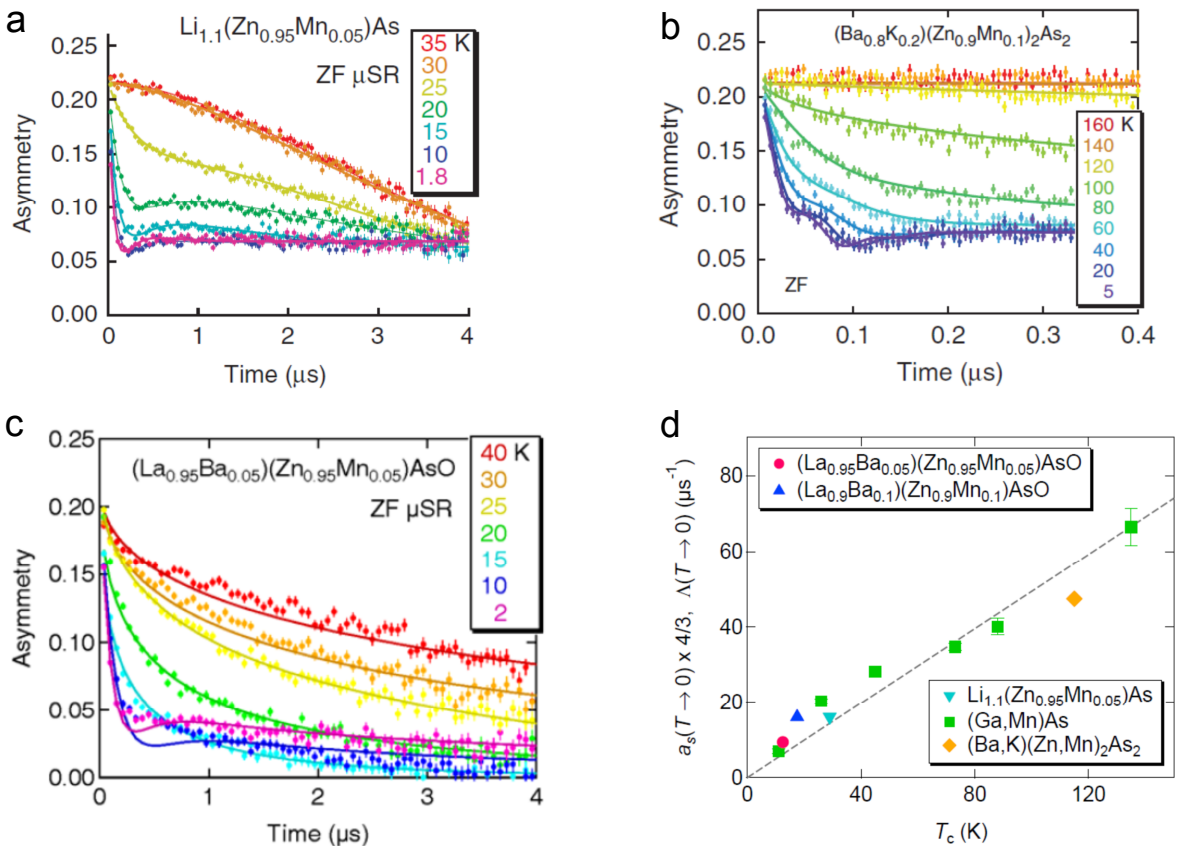

Fig. 3: Zero-field MuSR time results in novel DMS systems: the 111 (a; top left) [7], 122 (b; top right) [8], and 1111 systems (c; bottom left) [9]. The fast relaxation of ~ 2/3 of the full asymmetry followed by the slowly relaxing ~1/3 asymmetry indicates development of static magnetic order in the entire volume. (d; bottom right) Comparison of the initial decay rate at low temperatures in these three systems [7-9] and in (Ga,Mn)As [5]. (see [7-9] for color figures)

In all the three systems, we see fast relaxation of ~ 2/3 of the full asymmetry followed by the slowly relaxing ~1/3 asymmetry, which indicates development of static magnetic order in the entire volume.
Compared to the time spectra of the 111 and 122 systems (Fig. 3(a) and (b)), those of the 1111 system exhibit more pronounced signatures of relaxation due to dynamically fluctuating local fields, as discussed in details in ref. [9].

The rate of the initial fast relaxation at low temperatures provides a measure of static random internal field at the muon site, which is proportional to the static frozen component of individual Mn moments multiplied by the concentration in the dilute limit [11]. Figure 3(d) compares this parameter observed in the three new DMS systems with those in the conventional (Ga,Mn)As system [5]. A nearly linear trend found when plotted against the Curie temperature T_C of each system indicates that all these systems share the strength and mechanisms of ferromagnetic exchange interaction among dilute Mn moments.

4. Discussions, conclusions and outlook

These results demonstrate that novel DMS systems can be obtained by replacing Fe with (Zn,Mn) in many of the FeAs-based high-Tc superconductors. The difference in irreversibility and coercive field between the 111 and those of the 122 and 1111 DMS systems may be due to different crystal structures between cubic 111 and tetragonal 122 and 1111 systems.

In general, the history dependent behavior can be found both in many regular ferromagnets due to formation and motion of magnetic domains [12], and in spin glasses due to multiple minima of free energy as a function of spin configurations [13]. In some cases z-component of the spin behaves as ferromagnets while x- and y-components as spin gasses [13]. Detailed distinction of these three different cases requires not only the magnetization data but also neutron scattering results for spatial spin correlations. Since magnetic neutron scattering signal cannot be observed due to spatially dilute Mn moments and lack of single crystal specimens, there is no definite evidence at this moment to allow distinguishing between ferromagnetic and spin glass states for the present system.

Practically speaking, however, there is a clear difference between typical ferromagnets and spin glasses in their magnitudes of the saturation moment size in the ground state at low temperatures obtained in zero field after training in high external magnetic fields. In many ferromagnets, the remanent magnetization value is in the order of Bohr magneton per magnetic atom, while in typical
dilute-alloy spin glasses, it is 0.01 Bohr mangeton per magnetic atom or less [14,15]. In the 122 and 1111 DMS systems, this remanent magnetization is approximately 1 Bohr magneton per Mn, as shown in Fig. 1 and Fig. 2. Therefore, we tentatively assign these systems to ferromagnets rather than to spin glasses.

The so-called "spin glass relaxation function" [11] was used to fit the MuSR data shown in

Figs 3(a)-(c). This does not provide any distinction between ferromagnetic and spin glass systems, especially for the cases with spatially dilute magnetic moments. For example, the earlier MuSR results on conventional DMS system (Ga,Mn)As fitted quite well to the spin glass relaxation function [5], while accumulated studies, such as anomalous Hall effect, established that (Ga,Mn)As has ferromagnetic spin correlations below T_C, rather than random spin glass correlations.

As shown in Table 1 for the122 system, the semiconducting undoped compound, doped DMS systems, antiferromagnetic compounds with 100 % of Mn without Zn and the superconducting FeAs compound share identical crystal structure, with an excellent matching of the lattice constants in the 122 and 1111 DMS systems. This feature will be very helpful in future challenges to generate interfaces and multilayer devices of various combinations of these systems having different ground states. The present discoveries of these novel DMS systems might open a new field of designing novel spintronics devices taking advantage of this unique feature.

Although our initial attempts yielded only p-type DMS systems, compounds with different transitional metals or pnictogen elements may lead to development of n-type DMS materials. With such system, one might produce a transistor composed of both n- and p-type ferromagnetic DMS systems. Since there can be many combinations of atoms for such novel DMS systems, we are planning to resort to modern theoretical and computational methods, including dynamical mean field theory, local density approximation and quantum Monte Carlo methods, to predict most promising route towards materials with higher Curie temperatures as well as n-type carriers.

These novel DMS systems can be obtained as bulk specimens. This allows NMR and neutron scattering experiments. Successful NMR signals have been observed in Li(Cd,Mn)P and Li(Zn,Mn)As, while structural neutron studies have been performed in $(Ba,K)(Zn,Mn)_2As_2$. Development of single crystal specimens will further allow magnetic neutron scattering studies and possible carrier doping via application of gate voltage. These efforts are currently underway.

Table 1 | Crystal structures and lattice constants of superconducting $(Ba,K)Fe_2As_2$, antiferromagnetic $BaMn_2As_2$, semiconducting $BaZn_2As_2$ and ferromagnetic $(Ba,K)(Zn,Mn)_2As_2$.

Compound	$(Ba,K)Fe_2As_2$	$BaMn_2As_2$	$BaZn_2As_2$	$(Ba,K)(Zn,Mn)_2As_2$
Space group	I4/mmm	I4/mmm	I4/mmm	I4/mmm
a (Å)	3.917	4.169	4.121	4.131
c (Å)	13.297	13.473	13.575	13.481
Physical properties	Superconductor ($T_C = 38$ K)	Antiferromagnet ($T_N = 625$ K) semiconductor	Semiconductor	Ferromagnet ($T_C = 180$ K) semiconductor

Acknowledgement

The present work was supported by the Chinese NSF and Ministry of Science and Technology (MOST) through research projects at IOP; the National Basic Research Program of China (973 Program) under grant no.2011CBA00103 at IOP and Zhejiang; the US NSF PIRE (OISE-0968226) and DMR-1105961 projects at Columbia; the JAEA Reimei project at IOP, Columbia, PSI, McMaster and TU Munich; and NSERC and CIFAR at McMaster.

References

[1] Ohno, H. Making nonmagnetic semiconductors ferromagnetic. Science **281**, 951–956 (1998).

[2] Dietl, T. A ten-year perspective on dilute magnetic semiconductors and oxides. Nature Mater. **9**, 965–974 (2010).

[3] Zutic, I., Fabian, J. & Das Sarma, S. Spintronics: fundamentals and applications. Rev. Mod. Phys. **76**, 323–410 (2004).

[4] Masek, J. et al. Dilute moment n-type ferromagnetic semiconductor Li(Zn,Mn)As. Phys. Rev. Lett. **98**, 067202 (2007).

[5] Dunsiger, S. R. et al. Spatially homogeneous ferromagnetism of (Ga,Mn)As. Nature Mater. **9**, 299–303 (2010).

[6] Wang, X. C. et al. The superconductivity at 18K in LiFeAs system. Solid State Commun. **148**, 538–540 (2008).

[7] Deng, Z. et al., Li(Zn,Mn)As as a new generation ferromagnet based on a I–II–V semiconductor, Nature Communications **2**, 422 (2013): DOI: 10.1038/ncomms1425.

[8] Zhao, K. et al., New diluted ferromagnetic semiconductor with Curie temperature up to 180 K and isostructural to the '122' iron-based superconductors, Nature Communications **4**, 1442 (2013): DOI: 10.1038/ncomms2447.

[9] Ding, C. et al., $(La_{1-x}Ba_x)(Zn_{1-x}Mn_x)AsO$: A Two Dimensional "1111" Diluted Magnetic Semiconductor in Bulk Form, Phys. Rev. **B 88**, 041102(R) (2013).

[10] Deng, Z. et al., New diluted ferromagnetic semiconductor Li(Zn,Mn)P with decoupled charge and spin doping, submitted to Phys. Rev. **B** (2013).

[11] Uemura, Y. J., Yamazaki, T., Harshman, D. R., Senba, M. & Ansaldo, E. J. Muon-spin relaxation in AuFe and CuMn spin glasses. Phys. Rev. **B 31**, 546–563 (1985).

[12] see, for example, Jiles, D.C. and Atherton, D.L., Theory of ferromagnetic hysteresis, J. Magn. Magn. Matrs. **61**, 48-60 (1986).

[13] Fischer, K.H. and Hertz, J.A., *Spin Glasses*, Cambridge Univ. Press (1991).

[14] Tholence, J.L. and Tournier, R., Susceptibility and Remanent Magnetization of a Spin Glass, J. Phys. (Paris) **35**, C4-229 (1974).

[15] Prejean, J.J., Time and Temperature Evolution of a Saturated Thermoremenent Magnetization in a Spin Glass, J. Phys. (Paris) **39**, C6-907 (1978).

5. Initial Processes of Radiation Effects on Genomic Stability

Marie-Anne Hervé du Penhoat[1], Evelyne Sage[2], Chantal Houée-Lévin[3], Sandrine Lacombe[4], Marie-Françoise Politis[5], Alain Touati[1], Rodolphe Vuilleumier[6], Marie-Pierre Gaigeot[5], Riccardo Spezia[5], Frank Wien[7], Kentaro, Fujii[8], Naoya Shikazono[9], and Akinari Yokoya[8]

[1] Institut de Minéralogie et de Physique des Milieux Condensés, UMR 7590, Université Pierre et Marie Curie, France
[2] Laboratoire de Biologie des Radiations, Institut Curie, France
[3]Laboratoire de Chimie Physique, UMR 8000, Université Paris Sud, France
[4] Institut des Sciences Moléculaires d'Orsay, UMR 8214, Université Paris Sud, France
[5]Laboratoire Analyse et Modélisation pour la Biologie et l'Environnement, UMR 8587, Université d'Evry val d'Essonne, France
[6] Département de Chimie, Ecole Normale Supérieure, Paris
[7]SOLEIL Synchrotron, France
[8]Advance Science Research Center, Japan Atomic Energy Agency, Japan
[9]Quantum Beam Science Directorate, Japan Atomic Energy Agency, Japan

Abstract

We describe the progresses and current status of the REIMEI study on "Initial processes of radiation effects on genomic stability", which is a new collaborative project between France and Japan. The theoretical study on the fragmentation pattern of doubly ionized deoxyribose has reached a new stage focusing on the effect of water molecules surrounding the deoxyribose molecule. In order to substantiate the theoretical predictions, new devices have been installed in a SPring-8 beamline. To explore the origin of signal transduction of DNA repair processes, a preliminary CD measurement in the far UV region was performed to study histone conformation changes. Based on these results, we will propose a new experimental subject in SOLEIL synchrotron to investigate the conformational changes of phosphorylated histone. Preliminary experiments using mammalian cell free extract have also been performed focusing on the role of DNA polymerases on the mutagenic potential of clustered DNA lesions.

1. Research Objectives

It is well known that genomic stability of living organisms is seriously affected by ionizing radiation. To understand radiation effects has been recognized as one of very important subjects to not only provide practical aspects on low-dose effects of diagnostic radiation, radon absorption in buildings, or nuclear accidents such as seen in "Fukushima", but also to reveal evolution of life in terms of adaptation to radiation-stresses from the environment during geological age. The main purpose of our REIMEI project is to clarify the physicochemical processes of radiation effect on biomolecules and the biological responses to radiation damage

in cells. The project consists of three research lines (sub-projects) which have a common object concerning radiation effect on living cells and bio-molecular damage using spectroscopic and biochemical approaches.

2. Research Contents and Results

2.1 Sub-project 1: Theoretical study of DNA strand scission and its experimental verification

We have addressed the first sub-subject, how the atoms in the pentose ring of deoxyribose molecule are released by double ionization. Because the sugar moiety is a major component of the DNA chain, we expect to obtain one of the mechanisms of DNA-strand-breakage, which may be a part of the clustered DNA damage (see Sub-project 3) induced in cellular genomes exposed to ionizing radiation. In order to study radiation damage to deoxyribose molecules, we apply the theoretical approaches we have developped to investigate the fragmentation pattern of doubly ionized molecules in the condensed phase: *Ab* initio molecular dynamics (MD) calculations such as those based on time-dependent density functional theory (TDDFT) in femtosecond scale [1], or DFT-based Born-Oppenheimer (BO) dynamics in picosecond scale. Previously, doubly ionized deoxyribose was shown to undergo dissociation in the gas phase [2]. Based on these experimental evidences, our calculations have confirmed an ultrafast dissociation as shown in Fig. 1. The fragmentation depends on the local environment of the molecule and on the ionized orbital, but maybe not on the position of the K hole. Full electron quantum calculations of most probable channels of Auger deexcitation have to be done in future.

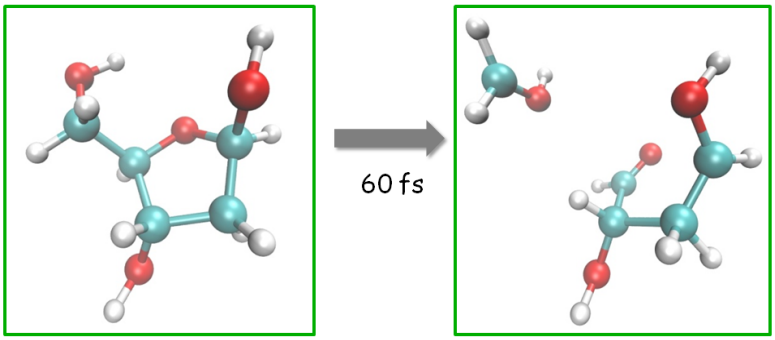

Fig. 1 Born-Oppenheimer dynamics of ground state deoxyribose^{2+} in gas phase. CH_3O^+ was reported by D.T. Ha et al. [2].

The next target of the TDDFT calculation is a deoxyribose molecule embedded in water molecules (H_2O) when ionized in O*1s* orbitals. Based on discussions on the experimental conditions, such as hydration of the deoxyribose molecule or temperature of sample films, we are now able to ensure realistic initial configurations (position and velocity of the atoms prior to ionization) from the theoretical side. We also constructed a nozzle system for water vapor exposure (Fig. 2) which was installed in the Japanese synchrotron, SPring-8, in November, 2012. We try to obtain experimental evidences of fragmentation pattern of deoxyribose molecule with two holes (following core ionization and Auger effect) induced by soft X-irradiation to compare them with the theoretical prediction. The preliminarly data of desorbed ion mass spectrum using a hydrated deoxyribose sample measured using a SPring-8 soft beamtime is

also shown in Fig. 2.

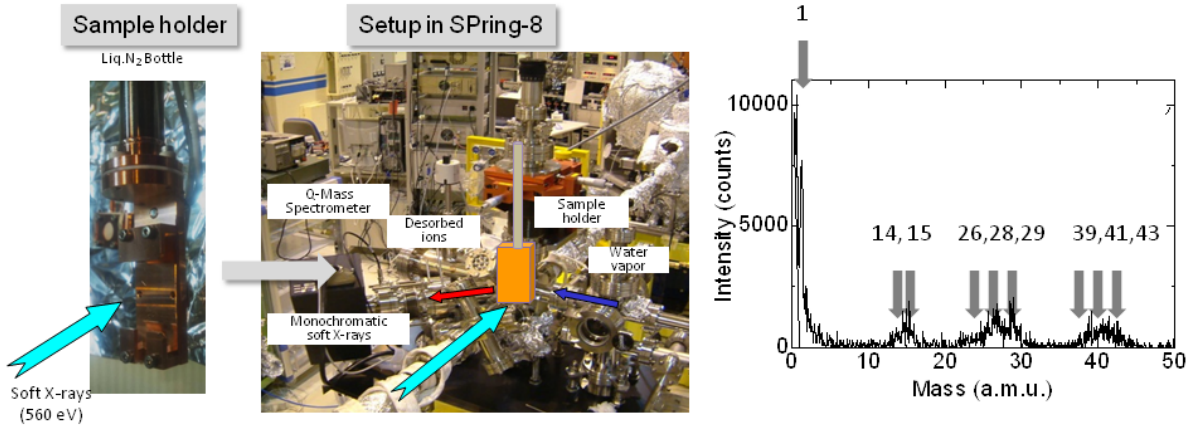

Fig. 2 Experimental setup of a Q-Mass spectrometer in SPring-8 and the mass spectrum observed using a hydrated deoxyribose film.

2.2 Sub-project 2: Biomolecular modifications explored by synchrotron spectroscopic techniques

It has been gradually recognized that a small fraction of surviving cells after low-dose of ionizing irradiation would transform to abnormal cells after normal cell divisions, potentially involved in carcinogenesis even though most of the DNA damage is rapidly repaired by enzymes (see Sub-project 3). These trans-generational effects are thought to be caused by modification of DNA binding proteins, such as phosphorylation of DNA binding proteins which are chromatin constituent factors. Another possibility yet unexplored is that the unrepaired oxidation induced by irradiation modifies the activity of proteins. However, there have been very few studies of protein modifications directly induced by irradiation, and also by cellular metabolism known as “epigenetic effects” so far. Thus we set of goals of the sub-project 2 to apply advanced spectroscopy techniques to observe the conformational change in a chromatin architecture induced by ionizing irradiation.

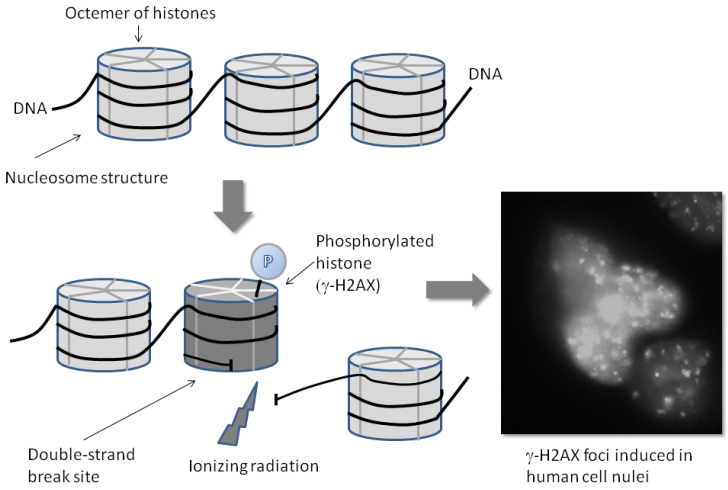

Fig. 3 Histone phosphorylation (histone γ-H2AX) is induced at DNA double strand break site produced by ionizing irradiation. The phosphorylation is thought to involve a change of the chromatine architecture which is a signal to recruit succeeding DNA repair protein machineries into the DSB site. The photograph shows foci of γ-H2AX indicated as dots in the cell nuclei of human cancer cells (Fucci-HeLa).

We focus on phosphorylation of histone proteins (Fig. 3). If DNA strand breaks (see Sub-project 1) arise proximately in both strands, the double helix is disrupted (double strand break (DSB)). DSB have been known to cause phosphorylation of histone proteins observed as histone γH2AX foci in a living cell. It has been suggested that the histone phosphorylation is a signal to recruit repair protein machineries into the DSB sites.

We have performed a feasibility study to examine the structural changes of chromatin by the histone phosphorylation using CD or ion mass spectroscopy (IMS). We have accumulated preliminary data using a conventional CD spectrometer to observe CD spectrum of histone H1 protein. The obtained spectra in the far UV region show dependence on conformational changes of the protein induced by conditional changes in the sample solution (Fig.4). Thus we further apply CD and IMS using French synchrotron, SOLEIL, beamlines supplying intense photon beam from UV to vacuum UV (VUV) region (130-250 nm). It is expected that the VUV light causes excitation much higher energy level than UV light. This might be to our advantage for studying a new aspect of the modifications of proteins or protein-DNA complex.

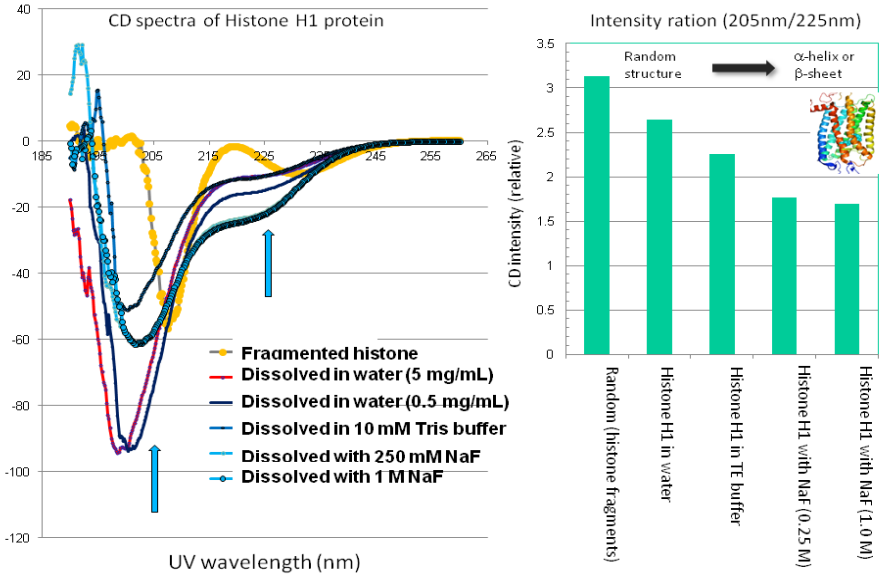

Fig. 4 Preliminary results of Circular Dichroism (CD) measurement for detection of conformational changes of histone protein H1 in the far UV energy region. The ratio of CD intensity at 205 nm to that at 225 nm depends on the sample conditions, indicating that the conformational changes of the histone from random structure to α-helix or β-sheet is detected as the change of CD signal.

2.3 Sub-project 3: DNA damage repair in eucaryotic and prokaryotic cells

The integrity of the genome of living organisms is continuously challenged. Cells have evolved to possess mechanisms that counteract these threats to genome integrity. The harmful effect of ionizing radiation has been proposed to largely result from clustered DNA damage, which likely is the only relevant DNA damage at low radiation doses. Both, the Japanese and the French labs contributed to demonstrate that clustered DNA lesions impair DNA repair processes and are highly mutagenic in bacteria and yeast or mammalian cells.

The aim of sub-project 3 is to provide a comprehensive view on the mutagenic potential of clustered damage in both eukaryotes (yeast or mammalian cells) and prokaryotes (bacteria). We have already performed preliminary experiments using mammalian cell free extract in October, 2012. Emphasize has been put on the role of DNA polymerases on the mutagenic potential of clustered DNA lesions (Fig. 5). We have prepared transfection of plasmid DNA carrying clustered lesions into yeast *Saccharomyces cerevisiae*, deficient or not in DNA polymerase activities, to analyze mutations (France), and into *E. coli*, deficient or not in DNA polymerase activities, to analyze.

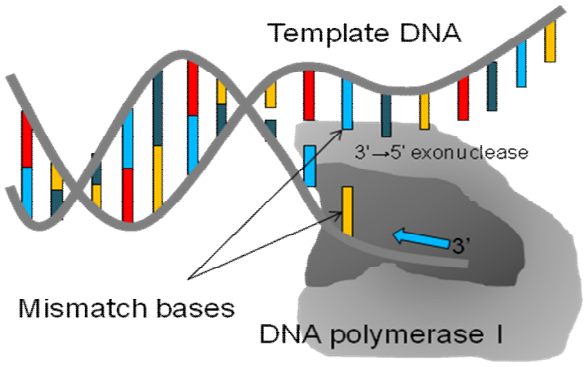

Fig. 5 Schematic drawing of DNA polymerase I editing mismatch bases induced in DNA by ionizing irradiaion.

3. Conclusion

The REIMEI project has been implemented since July 2012. Using the REIMEI budget, interexchange of scientists between France and Japan has been performed to discuss the detail of the project. We organized a workshop "Initial Processes of Radiation Effects on Genomic Stability" from March 13th to 24th at UPMC in Paris to report and discuss current statuses of each sub-projects. Some noteworthy progresses have been reported. Our project is unique and will contribute to understanding biological responses to radiation. We are going to further exchange of researchers, particularly young scientists including graduated students, between France and Japan to accelerate research activities as well as to keep international competitiveness in the new areas of research.

Acknowlegments

This work was granted access to the HPC resources of **CINES** and IDRIS under the allocation x2013085014 made by **GENCI** (Grand Equipement National de Calcul Intensif).

References

[1] P. Lopez-Tarifa et al., *Angewandte Chemie* **52**, 3160 (2013).

[2] D.T. Ha et al., Physical Review A **84**, 033419 (2011).

6. Studies of Exotic Modes of Fission in the Lead Region

Andrei Andreyev[1,2], Katsuhisa Nishio[2], Ichiro Nishinaka[2], Hiroyuki Makii[2], Kentaro Hirose[2], Hiroyuki Koura[2], Yutaka Utsuno[2], Shuya Ota[2], Satoshi Chiba[3], Victoria Truesdale[1], Lars Ghys[4], Tsutomu Ohtsuki[5]

[1] Department of Physics, University of York, York, UK
[2] Advanced Science Research Center, JAEA, Tokai, Japan
[3] Tokyo Institute of Technology, Tokyo, Japan
[4] KU Leueven, Leuven, Belgium
[5] Tohoku University, Japan

Abstract

In a series of complementary experiments at the tandem of JAEA and at the mass-separator ISOLDE (CERN), new fission phenomena in the lead region of the chart of nuclei were investigated. At ISOLDE, the low-energy fission of ^{194,196}Po was studied via the process of beta-delayed fission of the parent ^{194,196}At nuclei. A multi-modal fission fragment mass split was observed for ^{194,196}Po. At JAEA the higher-energy fusion-fission studies of ^{198}Hg, ^{191,193}Ir were performed in reactions with protons and ^{7}Li. In the JAEA experiment, we observed a transition from mass-symmetric to mass asymmetric fission between ^{189}Ir and ^{193}Ir. By studying fission in these regions, we investigate the new evolution of shell structure to regulate fission (as far as fission is concerned) of the chart of nuclides.

1. Introduction and Research Objectives

It is well known that low-energy fission data are notoriously difficult to obtain except for well-studied cases of spontaneous fission and particle-induced fission in the vicinity of beta-stability in the actinide region, see nuclei shown by open circles in Fig.1. However, in the last decade, through technological, experimental and theoretical advances, the situation in low-energy fission studies has changed dramatically. Nowadays, with the use of modern production and detection techniques we can obtain fission data for **new regions of nuclei (as far as fission is concerned)**, which is characterized by exotic values of proton-to-neutron ratio N/Z. The preferential asymmetric fission fragment mass split of actinide nuclei with N/Z ≈ 1.5−1.6 (e.g. ^{227}Ra, ^{236}U, ^{256}Fm in Fig. 1) is well understood due to the strong shell effects of the fission fragments in the vicinity of the doubly-magic ^{132}Sn (Z=50, N=82). In contrast to this, a transition to a predominantly symmetrical mass split was observed in the pre-actinide and light At-Ra nuclei with N / Z ≈1.38−1.40 (e.g. ^{209}Ra, ^{213}At in Fig. 1). The goal of our experiments is fission studies in two unexplored (by fission) regions of the nuclidic chart – see Reg. 1 and Reg. 2 of Fig. 1. In Reg.1 we use the process of beta-delayed fission to study ^{194,196}At at ISOLDE, while fusion-fission reactions are used at JAEA to access nuclei in Reg.2

2. Research contents and results.

2.1 Beta-delayed fission of ^{194,196}At at ISOLDE

The fission studies at ISOLDE (Reg.1 of Fig.1) aim at exotic process of *low-energy* βDF in extremely neutron-deficient nuclei in the lead region. This is a scarcely-studied region as far as fission is concerned, which is situated ~25 neutrons away from the β-stability line, and in which the nuclei do not undergo spontaneous fission (SF). In βDF, the excitation energy of the fissionning nuclei is limited by the Q_{EC} of the precursor parent, and does not exceed ~5 MeV in the actinides and ~11 MeV in the lead region [1,2]. In 2012, successful βDF studies of ^{194,196}At were performed at ISOLDE. A particular highlight from the 2012 ISOLDE experiments is a surprising triple-humped fission fragment mass distribution in βDF of ^{196}At (Fig.2). The ISOLDE experiments became possible following the successful development of the laser-ionized astatine beams and recently reported in Nature Communications [3].

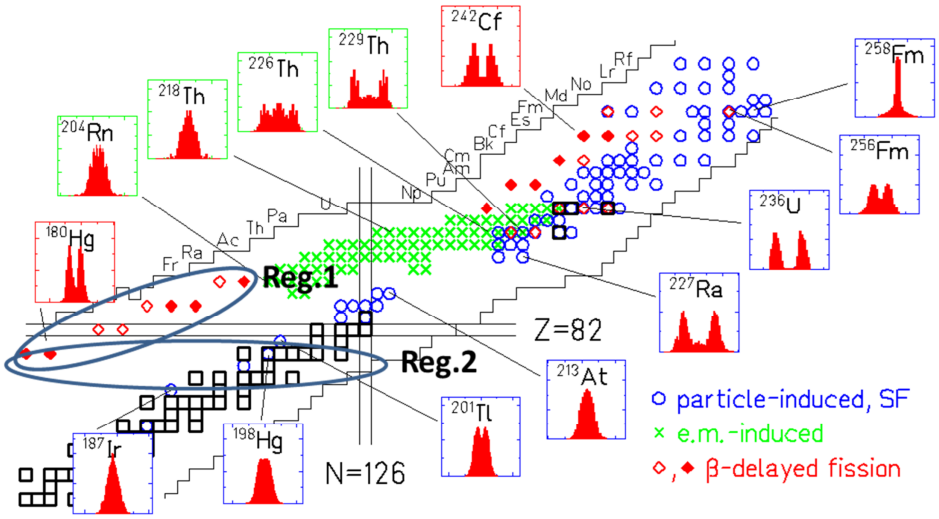

Fig 1. The map of nuclei in the Ir-Rf (Z=77-104) region with measured mass/charge distributions at **low** excitation energies, plot taken from [2]. Most of the data on the map have been collected for the "easier-accessible" pre-actinide and actinide nuclei. The particle-induced data are shown by open circles, the fission data from electromagnetically induced fission experiments at GSI are shown by crosses. The two regions of our interest are shown by ovals. The first region (Reg..1) of very neutron deficient nuclei with N/Z ≈ 1.2-1.3 includes ^{194,196}At studied in this work at ISOLDE. The second region (Reg.2) involves studies of ^{198}Hg, ^{191,193}Ir in fusion-fission reactions at JAEA.

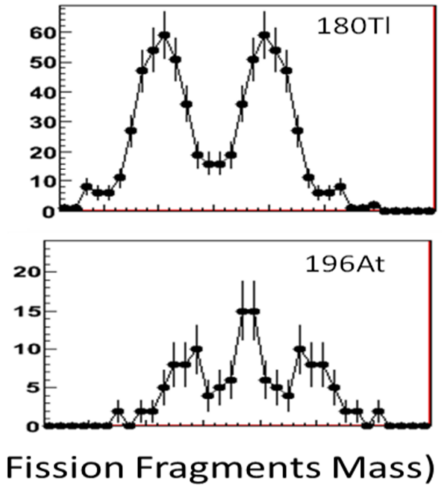

Fig.2 Contrasting fission fragment mass distributions for βDF of ^{180}Tl [1] and ^{196}At measured at ISOLDE. The ^{180}Tl data established a new (*second*) region of asymmetric fission in the Chart of Nuclides (Reg.1 in Fig.1). A clear transition from the asymmetric mass split of ^{180}Tl to a mixture of two fission modes – asymmetric and symmetric - is seen in in ^{196}At.

2. 2 Fusion-fission studies at JAEA tandem facility.

We also performed fission studies in the lead region at relatively higher excitation energies populated by heavy-ion induced fusion reactions. Advantage of this approach is that by choosing different combinations of projectile and target isotopes, wider variety of fissioning nuclei can be populated, allowing us to study systematic behavior of fission properties along the chart of nuclei. Moreover, by changing the beam energy, we can study the excitation energy dependence of the fission fragment mass distribution, and thus the transition from the low-energy fission influenced by the shell effects to the higher-energy fission where the symmetric liquid-drop behavior would be expected. For this study, we used the JAEA tandem facility at Tokai. The JAEA studies are unique and very important for this program, as we have access to a tandem accelerator (to reach the necessary beam energy precision when moving to deep sub-barrier energies) and also the JAEA fission group possesses a two-arm fission spectrometer used for many fission studies [4]. At the JAEA tandem facility, in-beam fission studies in the reactions of ^{7}Li + ^{182,186}W $\rightarrow$ ^{189,193}Ir* were carried out. We also investigated the reaction p + ^{197}Au leading to the compound nucleus, ^{198}Hg*. The fission fragment mass distributions for ^{198}Hg* were earlier measured by Itkis *et al.* [5]. This run was especially intended to cross-cpmapre our data and the data by Itkis *et al*,.

Figure 3 shows the fission fragment mass distributions in the reaction of p + ^{197}Au. Incident proton energy is 31.1 MeV. Our data shows the symmetric mass distribution, which agrees well with the data by Itkis obtained using the 30.0 MeV protons. Fragment mass distributions for ^{7}Li + ^{182}W $\rightarrow$ ^{189}Ir* are shown in Fig.4. Incident beam energy was changed to observe the excitation energy dependence of the fragment mass distributions. We also measured the mass distributions for ^{7}Li + ^{186}W $\rightarrow$ ^{193}Ir*. At the highest excitation energy, both for ^{189}Ir* and ^{193}Ir* show the symmetric mass distribution. The difference appears at the excitation energy of 41.5 MeV, at which the nucleus ^{193}Ir* fissions asymmetrically. The asymmetric fission becomes even

more pronounced at the lower excitation energy of 36.9 MeV. This is the first experiment to report the mass asymmetry in the fission of nuclei in such a low atomic number. Assuming that the N/Z ratio is conserved for the compound nucleus and fission fragments, the asymmetric peaks corresponds to ^{83}As (N=50) and ^{110}Ru(N=66). It seems, that the neutron shell at N=50 influences the mass split in the nucleus ^{193}Ir*. These results also establish the new region of asymmetric mass split on the chart of nuclei.

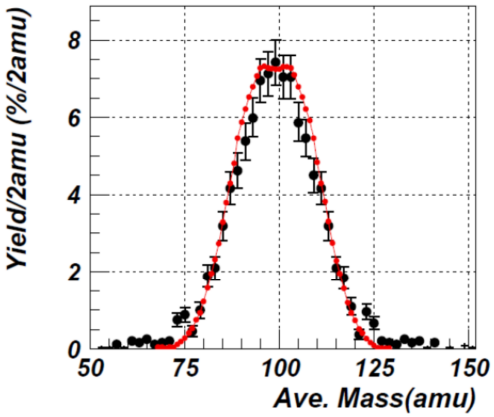

Figure 3 Fission fragment mass distribution of ^{198}Hg* produced in the reaction p + ^{197}Au. Present data are shown by black circles with error bar. The data connected by the red line is from [5].

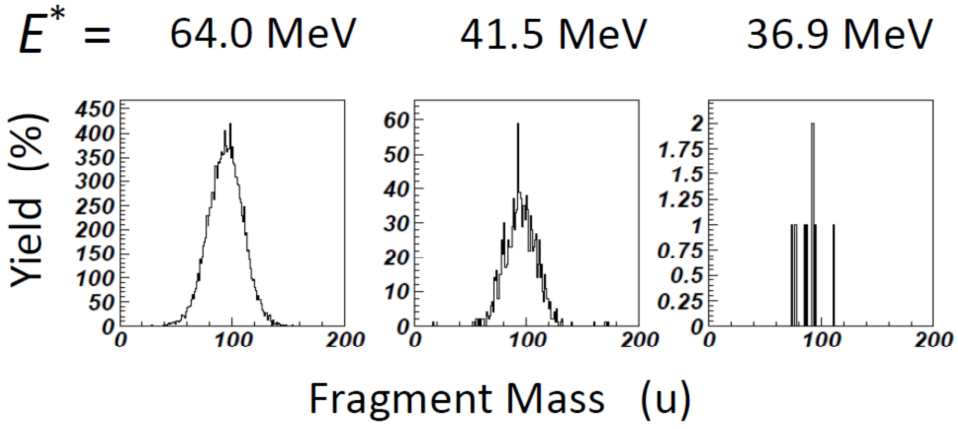

Figure 4 Fission fragment mass distributions of ^{189}Ir*. Excitation energies are shown.

3. Conclusion

In a series of ISOLDE experiments, β^+/EC delayed fission of ^{194,196}At was studied and multi-modal fission of their daughter products – isotopes ^{194,196}Po was observed. As the next step in the program, we will continue experiments for the β^+/EC-delayed fission of ^{186,188}Bi at ISOLDE. At the JAEA tandem facility, we observed an asymmetric fission at low energy in ^{193}Ir. This suggest the possible role of the neutron shell at N=50 for the nuclear rupture process. This

is the lightest element showing the asymmetric fission. It is found that transition from symmetric fission to asymmetric fission occurs in the iridium isotopes.

4. References

[1] A. Andreyev et al., "New type of asymmetric fission in proton-rich nuclei", Phys. Rev. Lett., **105**, 252102 (2010).

[2]. A. Andreyev, M. Huyse and P. Van Duppen, "Beta-delayed fission in atomic nuclei", Rev. Mod. Physics, vol. 85,1541, 2013.

[3] S. Rothe, A. Andreyev, K. Nishio et al, "Measurement of the first ionization potential of astatine by laser ionization spectroscopy" Nature Communications, 2819 (2013).

[4] K. Nishio *et al.*, Phys. Rev. C, **77**, 064607 (2008).

[5] Itkis et al., Sov. J. Nucl. Phys. **52**, 601 (1990).

7. Exploration of New Biological Specific Function by Heavy Elements Stimulus

Lynne Macaskie[1], Joanna Renshaw[2], Toshihiko Ohnuki[3], Norihiko Nishiguchi[4], Satoshi Utsunomiya[5], Yoshinori Suzuki[6], and Osamu Shirai[7]

[1]School of Biosciences, and [2]School of Geography, Earth and Environmental Sciences, University of Birmingham, UK
[3] Advanced Science Research Center, Japan Atomic Energy Agency, Japan
[4] Faculty of Engineering, Hokkaido University, Japan
[5] Department of Chemistry, Kyushu University, Japan
[6] School of Bioscience, Tokyo University of Technology, Japan
[7] Graduate School of Agriculture, Kyoto University, Japan

Abstract

We have carried out experiments to investigate bio-mineralization of rare earth elements (REE) on the cell surface of yeast *Saccharomyces cerevisiae*, and the bacteria *Bacillus subtilis*, *Pseudomonas fluorescens* and *Serratia* sp. The continuous removal of 1 mM La (100%) Nd (100%) and Eu (>80%) was observed using a continuous flow through immobilized *Serratia* sp cell columns. Chemical and physical characterization of bio-mineralized La and Eu was done by XRD at Birmingham and showed the formation of phosphate minerals. Additional cell column work using *S. cerevisiae, B. subtilis,* or *P. fluorescens*, showed that these bacteria are capable of bio-mineralizing Ce(III) and Sm(III). Chemical and physical characterizations of bio-transformed Ce and Sm were analyzed by JAEA, Kyushu U., Tokyo U. Tech. and Kyoto U. using XAFS, SEM and TEM. Results showed that Ce and Sm nanoparticles were formed. The high radiostability of the metal accumulating enzyme of *Serratia* sp. (which promotes metal phosphate deposition) was shown in whole cells, whereas pure enzyme lost its activity quickly under irradiation. Additional work on radionuclide (Cm) incorporation into *Serratia* sp calcium phosphate minerals (analogue for human bones) using EXAFS and Time Resolved Laser Fluorescence Spectroscopy (in collaboration with Karlsruhe Institute of Technology) showed that this actinide binds at the grain boundaries between crystallites, which has health implications for human exposure.

1. Research Objectives

The overall objective of the research is to explore new biological specific function and to understand this function in molecular level. To achieve this the aims are to use precious metals, actinides (An) and rare earth elements (REE) as stimuli, focusing particularly on cerium since Ce(III) and Ce(IV) are a surrogate for An(III) and An(IV), and Ce is also a REE in its own right. We aim to focus on bio-mineralization, even though many processes of transformation are

reported. Chemical and physical forms of the minerals formed by bio-transformations will be analyzed by JAEA, Kyushu U., Tokyo U. Tech., Kyoto U. by using XAFS, SEM, TEM, SANS, SAXS, EC, SEC-UVVis-RIM-ICPMS in order to find evidence of biological specific function for the transformation, and to elucidate the chemical processes responsible. In addition, we would like to apply the biological specific function to harness bioprocesses towards specific decontamination challenges resulting from the 2011 earthquake and tsunami.

2. Research Content

We used representative microorganism: yeast (*Saccharomyces cerevisiae*) and Gram positive (*Bacillus subtilis*) and Gram negative (*Pseudomonas fluorescens*, *Serratia* sp.) bacteria, 'simple' rare earth elements (Eu(III), Yb(III), Sm(III)) and multivalent ones (Ce(III)/IV)) as well as the radiotoxic actinide curium which exists predominantly as Cm(III). The microbiological systems were representative examples while the chemical systems comprised 'cold' REE surrogates for An(III)/(IV) as well as a real actinide Cm(III) for cross-validation. As well as examination of the underlying molecular mechanisms of metal removal into deposited biominerals and the physical and chemical nature of the metallic deposits, the work predicted continuous stability of the system by high-dose radioactive challenge experiments and by determination of the continuous removal of the REE 'surrogates' from aqueous flows using immobilized cells in a filter arrangement.

The surface of microorganisms, that is, the biomembrane, is composed mainly of phospholipids and membrane proteins. The phospholipids have phosphate groups that could bind metals. Here we also used a simplified model system, liposomes to investigate the understanding the adsorption behavior of lanthanide ions on a phospholipid membrane without any biological enzymatic activity.

After the Fukushima NPP accident, radioactive Cs was released in the environment. The interaction of Cs with microorganisms was therefore studied to estimate the potential impact of radioactive Cs to the environment.

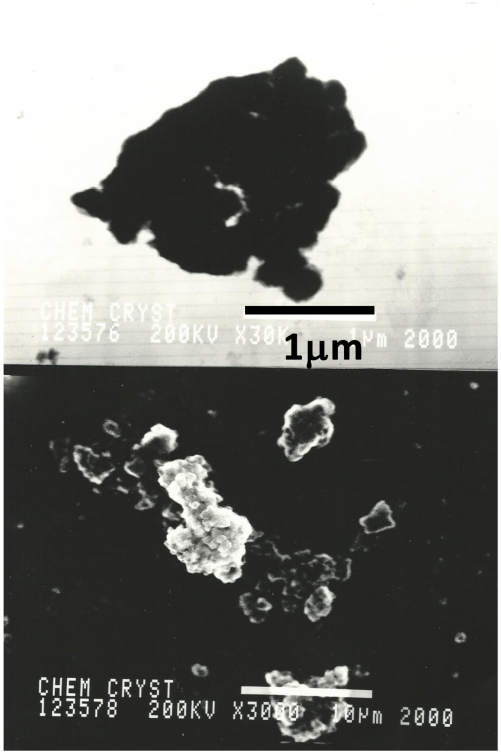

Fig. 1 TEM images of the precipitates formed on *Serratia* sp. after exposure to La(III) solution with added phosphate donor (5 mM glycerol 2-phosphate).

3. Research Results

Scoping tests using *Serratia* sp. showed high radiostability of the metal-depositing phosphatase which promotes metal phosphate deposition on the cells [2]. Phosphatases are

often very robust enzymes. Exposed to a commercial ^{60}Co gamma source purified phosphatase lost activity but whole-cell enzyme radiostability was seen after more than 1000 Gy, boosting confidence towards field applications over extended periods [2]. The same system was used to show continuous removal of 1 mM La (100%) Nd (100%) and Eu(>80%) from a continuous flow (pH 5.5) using cells immobilized as biofilm on reticulated foam sponge and supplemented with glycerol 2-phosphate (phosphate donor for the enzyme; 5 mM. La(III) was eventually removed to up to 10 times of the bacterial dry weight, with individual cells buried in crystalline precipitate (Fig. 1) identified as metal phosphate ($LaPO_4$) by XRD.

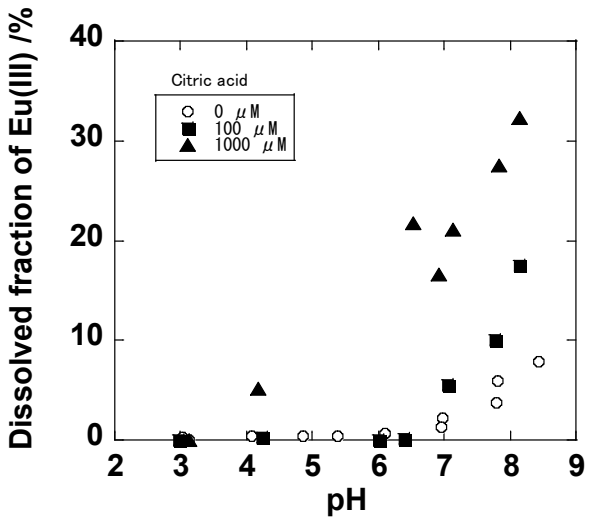

Fig. 2 The pH dependence of the dissolved fraction of Eu(III) in the presence of 167 ± 9 mg $_{dry\ weight}$ l^{-1} cells. The solutions contained 2 μM Eu(III), 0.1 M NaCl, 5 mM HEPES, and 0, 100 or 1000 μM citric acid. The aqueous phase was separated with a 0.20-μm membrane filter.

Further studies used *P. fluorescens*. In the presence of 100 μM citric acid, Eu(III) was almost completely sorbed on the cells below pH 7 (Fig. 2); Eu(III) sorption decreased by 2-8% compared to that in the absence of citric acid above pH 7. In the presence of 1000 μM citric acid, Eu(III) was completely sorbed on the cells at pH 3, and the sorption of Eu(III) decreased with a rise in pH. This decrease in Eu(III) sorption on *P. fluorescens* with an increase of citric-acid concentration suggests that citric acid competes for Eu(III) with functional groups on the cell's surface. The fall in Eu(III) sorption on the cells was significant at alkaline pH, suggesting that stability of Eu(III)-citrate complexes increases with a rise in pH, and this increasing tendency is greater than that of Eu(III)-cell-surface complexes. Thus, citric acid apparently reduces the sorption of trivalent actinides on microorganisms, especially at alkaline pHs, by forming stable complexes with them.

The surface of microorganisms, that is, the biomembrane, is composed mainly of phospholipids and membrane proteins. The phospholipids have phosphate groups. Here we used a simplified model system, liposome (Fig. 3), to investigate the adsorption behavior of lanthanide ions on a phospholipid membrane without any biological activity.

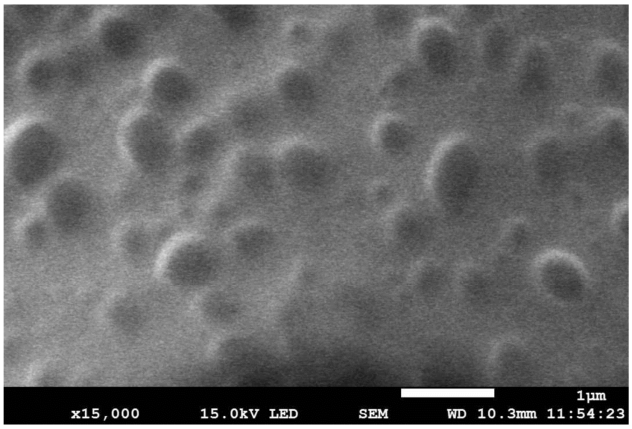

Fig. 3 SEM image of the liposome in ionic liquid

The adsorption behavior of lanthanide ions (except for Pm) on

liposomes composed of phosphatidyl- choline and cholesterol was examined to understand the interaction between lanthanide ions and the phosphoryl moiety of phospholipids [5]. The adsorption amount of lanthanide ions increased with an increase in pH in the weakly acidic condition. Selective adsorption with the local maximum at the Eu^{3+} ion and local minimum at the Er^{3+} ion was observed, similar to the selective adsorption of the bacterial cell surface, but different from that of orthophosphates. These results indicate that the adsorption of lanthanide on the phospholipid is not derived by simple adsorption on orthophosphate functional groups, but by the composition and molecular structure of the phospholipid. Our results strongly suggest that liposomes can be used as a simple biomembrane model without any biological activity for the study of adsorption of lanthanide ions.

When a 1 x 10^{-4} M Yb(III) solution was contacted with cells in the solution containing 1 g/L glycerol 2-phosphate and 1 x 10^{-3} M citric acid at pH 7, the soluble Yb(III) concentration decreased as a function of exposure time. Analysis of the cells by FESEM and XAFS showed that Yb(III) phosphate nanocrystals bearing with phosphate were formed on the cells by exposure to Yb(III) for 96 h. EXAFS analysis showed the formation of $YbPO_4$ mineral. Without glycerol-2-phosphate no precipitate was observed on *P. fluorescens* after exposure of Eu(III) in the presence of 1 mM citric acid at pH 7. These results indicate that *P. fluorescens* degraded glycerol-2-phosphate and the liberated P was reacted with Yb(III) on the cell surface, resulting in the formation of Yb(III) phosphate nanocrystallites as occurs with *Serratia* sp.

The time courses of the OD and the citric acid concentration, respectively, in media containing different Cs concentrations after the inoculation of *P. fluorescens* showed that in the absence of competing K^+ , the OD did not increase and the concentration of citric acid slightly decreased from 20 mM to 17 mM over 64 h. These results indicate that *P. fluorescens* cells did not grow in the absence of K^+ and that Cs^+ will not substitute for K^+ physiologically in this strain.

In the medium containing 0.1 mM KCl, the OD increased gradually to 0.28 and the citric acid concentration decreased to 0.23 mM for 64 h. In the media containing 1.0 and 10 mM KCl, the OD increased to 0.58 and 0.60, respectively, for 42 h, when the citric acid concentration decreased to below the detection limit, and then gradually decreased through 64 h. These results indicate that the cell growth was influenced by K^+ in the medium.

In contrast, the growth of *Rhodopseudomonas capsulata* cells is enhanced by 0.1 and 1.0 mM Cs^+ even in the absence of K. *R. capsulata* has a specific K^+ transporter (i.e. Kup), which shows low selectivity between K^+ and Cs^+ [6]. However, in this study, the presence of Cs^+ without K^+ did not result in the growth of *P. fluorescens* cells.

The amount of Cs accumulated increased from 1.8 to 4.2 μmol $Cs/g_{cell\ dry\text{-}weight}$ with a rise in the pH of the solution from 3.5 to 7.5 (Fig. 4). The final pHs were 3.5, 6.7, and 7.5, changing variously from their starting values of 3.0, 7.0, and 9.0, respectively. The *P. fluorescens* cells have carboxyl and phosphate functional groups on their surfaces. These functional groups deprotonate with increasing pH and consequently are free to associate with cations [8]. The pH dependence in the Cs^+ adsorption showed that the adsorption of Cs^+ occurred through the exchange with H^+ on functional groups of the cell surfaces of *P. fluorescens*. The adsorbed Cs was completely desorbed with within 24 h by 1 M CH_3COONH_4. A 1 M CH_3COONH_4 solution is

typically used as an extract solution to estimate the amount of the reversible cations in soils [5]. Thus, Cs^+ is reversibly adsorbed on the functional groups of the cell surfaces of *P. fluorescens*. The Cs^+ desorption rate was slower than the Cs^+ adsorption rate. Ohnuki [4] reported that the desorption and the adsorption rates were almost equivalent in the case of smectite. *P. fluorescens* has peptidoglycan layers on its cell walls, which consist of a cross-linked mesh structure [7]. The results suggest that adsorption of Cs^+ on the cell surfaces of *P. fluorescens* (membranes and peptidoglycan) differs from that on the reversible site in smectite.

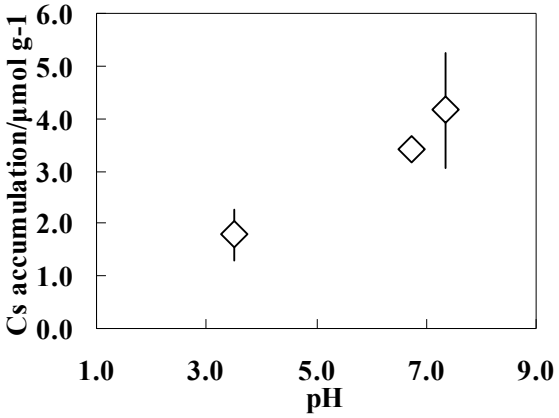

Fig. 4 Effect of pH on the accumulation of Cs by *P. fluorescens* cells. The final pHs are shown in the figure.

4. Conclusions

This study identifies the importance of biogenic metal phosphate deposition as an important, robust and durable method for removing radionuclides from solution using microbial 'filters' of several types. For high metal loads extra phosphate is supplied to the cells, but in other cases the cells require no extra feed and can generate biomineral precipitate from their own accumulated phosphate reserves. The importance of microorganisms in the migration of radioactive Cs is shown in the adsorption on the cell surface and tighter association of Cs with cell surface than clay mineral of smectite have been revealed using the microbial model systems.

5. Acknowledgements

We acknowledge with thanks the collaboration and input of Dr K. Holliday of Karlsruhre Institute of Technology, Germany, the UK 'FENAC' facility for solid state analysis.

6. References

[1] S. Yamasaki, et al., Chemistry Letters, **42**, 819 (2013).
[2] M. Paterson-Beedle et al. *Biotech Bioeng* , 109, 1937(2012).
[3] M. Jiang et al. *Chem Geol,* **277**, 61(2010).
[4] T. Ohnuki and N. Kozai, Radiochimica Acta, **66/67**, 327 (1994).
[5] C.J. Schollenberger and R.H Simon, Soil Sci. **59**, 13. (1945).
[6] P. Jasper, J. Bacteriol. **133**, 1314 (1978).
[7] T.J. Beveridge and S.F. Koval, Appl. Environ. Microbiol. **42**, 325 (1981).
[8] V.R. Phoenix et al Appl. Environ. Microbiol. **68**, 4827 (2002).

This is a blank page.

国際単位系（SI）

表１．SI 基本単位

基本量	SI 基本単位	
	名称	記号
長さ	メートル	m
質量	キログラム	kg
時間	秒	s
電流	アンペア	A
熱力学温度	ケルビン	K
物質量	モル	mol
光度	カンデラ	cd

表２．基本単位を用いて表されるSI組立単位の例

組立量	SI 基本単位	
	名称	記号
面積	平方メートル	m^2
体積	立法メートル	m^3
速さ，速度	メートル毎秒	m/s
加速度	メートル毎秒毎秒	m/s^2
波数	毎メートル	m^{-1}
密度，質量密度	キログラム毎立方メートル	kg/m^3
面積密度	キログラム毎平方メートル	kg/m^2
比体積	立方メートル毎キログラム	m^3/kg
電流密度	アンペア毎平方メートル	A/m^2
磁界の強さ	アンペア毎メートル	A/m
量濃度(a)，濃度	モル毎立方メートル	mol/m^3
質量濃度	キログラム毎立法メートル	kg/m^3
輝度	カンデラ毎平方メートル	cd/m^2
屈折率(b)	（数字の） 1	1
比透磁率(b)	（数字の） 1	1

(a) 量濃度（amount concentration）は臨床化学の分野では物質濃度（substance concentration）ともよばれる。
(b) これらは無次元量あるいは次元１をもつ量であるが、そのことを表す単位記号である数字の１は通常は表記しない。

表３．固有の名称と記号で表されるSI組立単位

組立量	SI 組立単位			
	名称	記号	他のSI単位による表し方	SI基本単位による表し方
平面角	ラジアン(b)	rad	1 (b)	m/m
立体角	ステラジアン(b)	sr(c)	1 (b)	m^2/m^2
周波数	ヘルツ(d)	Hz		s^{-1}
力	ニュートン	N		m kg s^{-2}
圧力，応力	パスカル	Pa	N/m^2	m^{-1} kg s^{-2}
エネルギー，仕事，熱量	ジュール	J	N m	m^2 kg s^{-2}
仕事率，工率，放射束	ワット	W	J/s	m^2 kg s^{-3}
電荷，電気量	クーロン	C		s A
電位差（電圧），起電力	ボルト	V	W/A	m^2 kg s^{-3} A^{-1}
静電容量	ファラド	F	C/V	m^{-2} kg^{-1} s^4 A^2
電気抵抗	オーム	Ω	V/A	m^2 kg s^{-3} A^{-2}
コンダクタンス	ジーメンス	S	A/V	m^{-2} kg^{-1} s^3 A^2
磁束	ウエーバ	Wb	Vs	m^2 kg s^{-2} A^{-1}
磁束密度	テスラ	T	Wb/m^2	kg s^{-2} A^{-1}
インダクタンス	ヘンリー	H	Wb/A	m^2 kg s^{-2} A^{-2}
セルシウス温度	セルシウス度(e)	℃		K
光束	ルーメン	lm	cd sr(c)	cd
照度	ルクス	lx	lm/m^2	m^{-2} cd
放射性核種の放射能(f)	ベクレル(d)	Bq		s^{-1}
吸収線量, 比エネルギー分与, カーマ	グレイ	Gy	J/kg	m^2 s^{-2}
線量当量, 周辺線量当量, 方向性線量当量, 個人線量当量	シーベルト(g)	Sv	J/kg	m^2 s^{-2}
酸素活性	カタール	kat		s^{-1} mol

(a)SI接頭語は固有の名称と記号を持つ組立単位と組み合わせても使用できる。しかし接頭語を付した単位はもはやコヒーレントではない。
(b)ラジアンとステラジアンは数字の１に対する単位の特別な名称で、量についての情報をつたえるために使われる。実際には、使用する時には記号radおよびsrが用いられるが、習慣として組立単位としての記号である数字の１は明示されない。
(c)測光学ではステラジアンという名称と記号srを単位の表し方の中に、そのまま維持している。
(d)ヘルツは周期現象についてのみ、ベクレルは放射性核種の統計的過程についてのみ使用される。
(e)セルシウス度はケルビンの特別な名称で、セルシウス温度を表すために使用される。セルシウス度とケルビンの単位の大きさは同一である。したがって、温度差や温度間隔を表す数値はどちらの単位で表しても同じである。
(f)放射性核種の放射能（activity referred to a radionuclide）は、しばしば誤った用語で"radioactivity"と記される。
(g)単位シーベルト（PV,2002,70,205）についてはCIPM勧告2（CI-2002）を参照。

表４．単位の中に固有の名称と記号を含むSI組立単位の例

組立量	SI 組立単位		
	名称	記号	SI 基本単位による表し方
粘度	パスカル秒	Pa s	m^{-1} kg s^{-1}
力のモーメント	ニュートンメートル	N m	m^2 kg s^{-2}
表面張力	ニュートン毎メートル	N/m	kg s^{-2}
角速度	ラジアン毎秒	rad/s	m m^{-1} s^{-1}=s^{-1}
角加速度	ラジアン毎秒毎秒	rad/s^2	m m^{-1} s^{-2}=s^{-2}
熱流密度，放射照度	ワット毎平方メートル	W/m^2	kg s^{-3}
熱容量，エントロピー	ジュール毎ケルビン	J/K	m^2 kg s^{-2} K^{-1}
比熱容量，比エントロピー	ジュール毎キログラム毎ケルビン	J/(kg K)	m^2 s^{-2} K^{-1}
比エネルギー	ジュール毎キログラム	J/kg	m^2 s^{-2}
熱伝導率	ワット毎メートル毎ケルビン	W/(m K)	m kg s^{-3} K^{-1}
体積エネルギー	ジュール毎立方メートル	J/m^3	m^{-1} kg s^{-2}
電界の強さ	ボルト毎メートル	V/m	m kg s^{-3} A^{-1}
電荷密度	クーロン毎立方メートル	C/m^3	m^{-3} sA
表面電荷	クーロン毎平方メートル	C/m^2	m^{-2} sA
電束密度，電気変位	クーロン毎平方メートル	C/m^2	m^{-2} sA
誘電率	ファラド毎メートル	F/m	m^{-3} kg^{-1} s^4 A^2
透磁率	ヘンリー毎メートル	H/m	m kg s^{-2} A^{-2}
モルエネルギー	ジュール毎モル	J/mol	m^2 kg s^{-2} mol^{-1}
モルエントロピー, モル熱容量	ジュール毎モル毎ケルビン	J/(mol K)	m^2 kg s^{-2} K^{-1} mol^{-1}
照射線量（X線及びγ線）	クーロン毎キログラム	C/kg	kg^{-1} sA
吸収線量率	グレイ毎秒	Gy/s	m^2 s^{-3}
放射強度	ワット毎ステラジアン	W/sr	m^4 m^{-2} kg s^{-3}=m^2 kg s^{-3}
放射輝度	ワット毎平方メートル毎ステラジアン	$W/(m^2$ sr)	m^2 m^{-2} kg s^{-3}=kg s^{-3}
酵素活性濃度	カタール毎立方メートル	kat/m^3	m^{-3} s^{-1} mol

表５．SI 接頭語

乗数	接頭語	記号	乗数	接頭語	記号
10^{24}	ヨタ	Y	10^{-1}	デシ	d
10^{21}	ゼタ	Z	10^{-2}	センチ	c
10^{18}	エクサ	E	10^{-3}	ミリ	m
10^{15}	ペタ	P	10^{-6}	マイクロ	μ
10^{12}	テラ	T	10^{-9}	ナノ	n
10^9	ギガ	G	10^{-12}	ピコ	p
10^6	メガ	M	10^{-15}	フェムト	f
10^3	キロ	k	10^{-18}	アト	a
10^2	ヘクト	h	10^{-21}	ゼプト	z
10^1	デカ	da	10^{-24}	ヨクト	y

表６．SIに属さないが、SIと併用される単位

名称	記号	SI 単位による値
分	min	1 min=60s
時	h	1h =60 min=3600 s
日	d	1 d=24 h=86 400 s
度	°	1°=(π/180) rad
分	’	1’=(1/60)°=(π/10800) rad
秒	”	1”=(1/60)’=(π/648000) rad
ヘクタール	ha	$1ha=1hm^2=10^4m^2$
リットル	L, l	$1L=11=1dm^3=10^3cm^3=10^{-3}m^3$
トン	t	$1t=10^3$ kg

表７．SIに属さないが、SIと併用される単位で、SI単位で表される数値が実験的に得られるもの

名称	記号	SI 単位で表される数値
電子ボルト	eV	$1eV=1.602\ 176\ 53(14)\times10^{-19}J$
ダルトン	Da	$1Da=1.660\ 538\ 86(28)\times10^{-27}kg$
統一原子質量単位	u	1u=1 Da
天文単位	ua	$1ua=1.495\ 978\ 706\ 91(6)\times10^{11}m$

表８．SIに属さないが、SIと併用されるその他の単位

名称	記号	SI 単位で表される数値
バール	bar	1 bar=0.1MPa=100kPa=10^5Pa
水銀柱ミリメートル	mmHg	1mmHg=133.322Pa
オングストローム	Å	1 Å=0.1nm=100pm=10^{-10}m
海里	M	1 M=1852m
バーン	b	$1\ b=100fm^2=(10^{-12}cm)2=10^{-28}m^2$
ノット	kn	1 kn=(1852/3600)m/s
ネーパ	Np	SI単位との数値的な関係は、対数量の定義に依存。
ベル	B	
デジベル	dB	

表９．固有の名称をもつCGS組立単位

名称	記号	SI 単位で表される数値
エルグ	erg	$1\ erg=10^{-7}$ J
ダイン	dyn	$1\ dyn=10^{-5}$N
ポアズ	P	1 P=1 dyn s cm^{-2}=0.1Pa s
ストークス	St	1 St =$1cm^2$ s^{-1}=$10^{-4}m^2$ s^{-1}
スチルブ	sb	1 sb =1cd cm^{-2}=10^4cd m^{-2}
フォト	ph	1 ph=1cd sr cm^{-2} 10^4lx
ガル	Gal	1 Gal =1cm s^{-2}=$10^{-2}ms^{-2}$
マクスウェル	Mx	1 Mx = 1G cm^2=10^{-8}Wb
ガウス	G	1 G =1Mx cm^{-2} =10^{-4}T
エルステッド(c)	Oe	1 Oe≙ $(10^3/4\pi)$A m^{-1}

(c) ３元系のCGS単位系とSIでは直接比較できないため、等号「 ≙ 」は対応関係を示すものである。

表10．SIに属さないその他の単位の例

名称	記号	SI 単位で表される数値
キュリー	Ci	$1\ Ci=3.7\times10^{10}Bq$
レントゲン	R	$1\ R = 2.58\times10^{-4}C/kg$
ラド	rad	$1\ rad=1cGy=10^{-2}Gy$
レム	rem	$1\ rem=1\ cSv=10^{-2}Sv$
ガンマ	γ	1γ=1 nT=10-9T
フェルミ		1フェルミ=1 fm=10-15m
メートル系カラット		1メートル系カラット = 200 mg = 2×10-4kg
トル	Torr	1 Torr = (101 325/760) Pa
標準大気圧	atm	1 atm = 101 325 Pa
カロリー	cal	1cal=4.1858J（「15℃」カロリー），4.1868J（「IT」カロリー）4.184J（「熱化学」カロリー）
ミクロン	μ	1 μ =1μm=10^{-6}m

（第8版，2006年改訂）

この印刷物は再生紙を使用しています